Circulation Research

ORIGINAL RESEARCH

Deacetylation of Septin4 by SIRT2 (Silent Mating Type Information Regulation 2 Homolog-2) Mitigates Damaging of Hypertensive Nephropathy

Ying Zhang, Naijin Zhang, Yuanming Zou, Chunyu Song, Kexin Cao, Boquan Wu, Shilong You, Saien Lu, Dong Wang, Jiaqi Xu, Xinyue Huang, Pengyu Zhang, Zihao Fan, Jingwei Liu, Zhongyi Cheng, Zhe Zhang, Chuize Kong, Liu Cao, Yingxian Sun

BACKGROUND: Hypertension can lead to podocyte damage and subsequent apoptosis, eventually resulting in glomerulosclerosis. Although alleviating podocyte apoptosis has clinical significance for the treatment of hypertensive nephropathy, an effective therapeutic target has not yet been identified. The function of septin4, a proapoptotic protein and an important marker of organ damage, is regulated by post-translational modification. However, the exact role of septin4 in regulating podocyte apoptosis and its connection to hypertensive renal damage remains unclear.

METHODS: We investigated the function and mechanism of septin4 in hypertensive nephropathy to discover a theoretical basis for targeted treatment. Mouse models including Rosa 26 (Gt(ROSA)26Sor)-*SIRT2* (silent mating type information regulation 2 homolog-2)-Flag-TG (transgenic) (*SIRT2*-TG) mice *SIRT2*-knockout, and *septin4*-K174Q mutant mice, combined with proteomic and acetyl proteomics analysis, followed by multiple molecular biological methodologies, were used to demonstrate mechanisms of SIRT2-mediated deacetylation of septin4-K174 in hypertensive nephropathy.

RESULTS: Using transgenic *septin4*-K174Q mutant mice treated with the antioxidant Tempol, we found that hyperacetylation of the K174 site of septin4 exacerbates Ang II (angiotensin II)– induced hypertensive renal injury resulting from oxidative stress. Proteomics and Western blotting assays indicated that septin4-K174Q activates the cleaved-PARP1 (poly [ADP-ribose] polymerase family, member 1)-cleaved-caspase3 pathway. In septin4-knockdown human renal podocytes, septin4-K174R, which mimics deacetylation at K174, rescues podocyte apoptosis induced by Ang II. Immunoprecipitation and mass spectrometry analyses identified SIRT2 as a deacetylase that interacts with the septin4 GTPase domain and deacetylates septin4-K174. In *Sirt2*-deficient mice and SIRT2-knockdown renal podocytes, septin4-K174 remains hyperacetylated and exacerbates hypertensive renal injury. By contrast, in Rosa26-*Sirt2*-Flag (*SIRT2*-TG) mice and SIRT2-knockdown renal podocytes reexpressing wild-type SIRT2, septin4-K174 is hypoacetylated and mitigates hypertensive renal injury.

CONCLUSIONS: Septin4, when activated through acetylation of K174 (K174Q), promotes hypertensive renal injury. Septin4-K174R, which mimics deacetylation by SIRT2, inhibits the cleaved-PARP1-cleaved-caspase3 pathway. Septin4-K174R acts as a renal protective factor, mitigating Ang II–induced hypertensive renal injury. These findings indicate that septin4-K174 is a potential therapeutic target for the treatment of hypertensive renal injury.

GRAPHIC ABSTRACT: A graphic abstract is available for this article.

Key Words: apoptosis ■ hypertensive nephropathy ■ podocytes ■ proteomics ■ sirtuins

Meet the First Author, see p 543 | Editorial, see p 625

Correspondence to: Yingxian Sun, MD, PhD, Department of Cardiology, the First Hospital of China Medical University, 115 Nanjing N St, Heping District, Shenyang, 110001 Liaoning Province, People's Republic of China, Email yxsun@cmu.edu.cn or Liu Cao, MD, PhD, College of Basic Medical Science, China Medical University; Key Laboratory of Medical Cell Biology, Ministry of Education, China Medical University; Liaoning Province Collaborative Innovation Center of Aging Related Disease Diagnosis and Treatment and Prevention, China Medical University, 77 Puhe Rd, Shenbei New District, Shenyang, 110001 Liaoning Province, People's Republic of China, Email lcao@cmu.edu.cn or Naijin Zhang, MD, PhD, Department of Cardiology, the First Hospital of China Medical University, 155 Nanjing N St, Heping District, Shenyang, 110001 Liaoning Province, People's Republic of China; Institute of health sciences, China Medical University; Key Laboratory of Reproductive and Genetic Medicine, National Health Commission, China Medical University, 77 Puhe Rd, Shenbei New District, Shenyang, 110001 Liaoning Province, People's Republic of China, Email njzhang@cmu.edu.cn
*Y. Zhang and N. Zhang contributed equally as first authors
Supplemental Material is available at https://www.ahajournals.org/doi/suppl/10.1161/CIRCRESAHA.122.321591.
For Sources of Funding and Disclosures, see page 623.

ORIGINAL RESEARCH

Novelty and Significance

What Is Known?

- Kidney is the primary organ of hypertension-induced targeted injuries. Hypertension damages and causes subsequent apoptosis of podocytes which form the final filtration barrier of glomeruli, resulting in irreversible glomerulosclerosis.
- The degree of podocyte damage and apoptosis is the key prognostic factor of renal disease, therefore, reducing podocyte apoptosis has potential significance in the treatment of hypertensive nephropathy.
- Septin4, as a proapoptotic protein, plays a crucial role in regulating caspase activation and is an important biomarker of organ damage.

What New Information Does This Article Contribute?

- The NAD-dependent deacetylase SIRT2 (silent mating type information regulation 2 homolog-2) helps protect the kidney from Angiotensin II-induced hypertensive renal injury.
- SIRT2-mediated deacetylation of the K174 residue of septin4 represses the PARP1 (poly [ADP-ribose] polymerase family, member 1)-cleaved-caspase3 pathway, which protects renal podocytes from hypertension and alleviates glomerulosclerosis.
- Septin4-k174 mitigates angiotensin II–induced renal injury and is a potential therapeutic target for the treatment of hypertensive nephropathy.

Damage to podocytes and subsequent apoptosis lead to irreversible glomerulosclerosis in patients with hypertension. Reducing podocyte apoptosis has potential significance in the treatment of hypertensive nephropathy. In this study, we found a novel and critical role for the regulation of the SIRT2-septin4 deacetylation axis in overcoming oxidative stress and inhibiting apoptosis of renal podocytes, hence reducing glomerulosclerosis and protecting against hypertensive kidney injury. We demonstrated that SIRT2 can protect the kidney from angiotensin II–induced hypertensive renal injury. SIRT2 interacts with the septin4 GTPase domain and deacetylates septin4-K174. Proteomic and Western blotting assays indicated that septin4-K174Q activates the cleaved-PARP1-cleaved-caspase3 pathway, exacerbating hypertensive renal injury. In septin4-knockdown human renal podocytes, septin4-K174R, which mimics deacetylation at K174, rescues hypertensive podocyte apoptosis. Angiotensin II–induced renal injury can be mitigated by targeting septin4-k174, which makes it a potential therapeutic target for hypertensive nephropathy.

Nonstandard Abbreviations and Acronyms

8-oxo-dG	8-oxo-2'-deoxyguanosine
Ang II	angiotensin II
CBP	CREB binding protein
PARP1	poly (ADP-ribose) polymerase family, member 1
SIRT2	silent mating type information regulation 2 homolog-2
UPCR	urinary protein creatinine ratio

Hypertension affects >1 billion people worldwide[1] and can induce a series of damaging effects on target organs. The GBD (Global Burden of Disease Study) 2017 states that the kidney is one of the main target organs damaged by hypertension. The global prevalence of hypertension-induced chronic nephropathy exceeds 23.6 million,[2] which significantly affects patients' survival time. Hypertension causes damage and subsequent apoptosis of podocytes,[3] which form the final filtration barrier of glomeruli,[4] eventually leading to glomerulosclerosis.[4–6] The degree of podocyte damage and apoptosis is regarded as the main prognostic factor of renal disease.[5] Alleviating podocyte apoptosis has potential clinical significance for the treatment of hypertensive nephropathy. Although some progress has been made in understanding the pathogenesis of podocyte apoptosis, a method of inhibiting podocyte apoptosis has not yet been discovered. A detailed study of the molecular mechanism and pathway of podocyte apoptosis is needed to develop a targeted treatment for hypertensive nephropathy.

Septin4 plays a key role in regulating caspase activation and apoptosis.[7] Septin4 belongs to the septin family and contains a highly conserved P-loop motif (GESGLGKS) located in the GTPase domain. The P-loop motif is essential for the apoptotic function of septin4.[7] Once caspase is activated and the induction of apoptosis factors occurs,[7,8] Septin4 then promotes the release of a series of cytokines[9,10] and amplifies the caspase cascade to induce apoptosis.[9] Septin4, therefore, functions as a proapoptotic protein and is an important marker protein for organ damage. The accumulation of pathogenic septin4 in the brain's dopaminergic cells can lead to cell death and development

of Parkinson disease.[11] However, inhibiting the expression of septin4 can decrease hypoxia-induced cardiomyocyte apoptosis[12] and alleviate anoxia/reoxygenation (A/R)-induced cardiomyocyte dysfunction.[13] Despite its role as a proapoptotic protein, no report to date has implicated septin4 in hypertensive renal damage.

Deacetylase activity has been linked to oxidative stress and apoptosis. Although post-translational modification (PTM) plays an important role in the apoptotic function of septin4,[14–16] whether septin4 is regulated by acetylation is not known. Sir2 (silent information regulator 2; called SIRT2 [silent mating type information regulation 2 homolog-2] in *Homo sapiens*), was first identified in yeast and belongs to the sirtuin family of nicotinamide adenine dinucleotide (NAD+)-dependent deacetylases and possesses histone deacetylase activity.[17,18] SIRT2 deacetylates substrates involved in diverse pathways. Decreased expression of SIRT2 can promote transcriptional activation of several apoptosis-related genes, which can increase apoptosis of cardiomyocytes.[19] Similarly, inhibition of SIRT2 can induce oxidative stress-triggered apoptosis to fight tumors.[20] Moreover, SIRT2 deficiency increases oxidative stress and further induces apoptosis.[21] SIRT2 function plays a key protective role in oxidative stress-heart failure, protecting the heart from Ang II (angiotensin II)–induced hypertrophic stimuli through its function as a histone deacetylase.[22,23] Given this key role of the SIRT2 deacetylase in oxidative stress and apoptosis, it is important to determine if deacetylation of septin4 via SIRT2 has a biological function in hypertensive renal injury.

Here, we provide the first evidence that septin4 can be acetylated. Moreover, we find that the NAD-dependent deacetylase SIRT2 helps protect the kidney from Ang II–induced hypertensive renal injury. SIRT2-mediated deacetylation of the K174 residue of septin4 represses the PARP1 (poly [ADP-ribose] polymerase family, member 1)-cleaved-caspase3 pathway, which protects renal podocytes from hypertension and alleviates glomerulosclerosis, an event associated with hypertensive kidney damage. Our findings describe a novel and critical role for the regulation of the SIRT2-septin4 deacetylation axis in inhibiting apoptosis and overcoming oxidative stress to protect against hypertensive kidney injury.

METHODS

Data Availability

The detailed experimental materials, methods, and data supporting the findings of this study are available within the article and its Supplemental Material. Raw data are available from the corresponding author upon reasonable request. The Major Resources Table is provided in the Supplemental Material.

RESULTS

SIRT2 Affects Ang II–Induced Renal Podocyte Apoptosis Through Interaction With the GTPase Domain of the Proapoptosis Protein Septin4

We examined the expression profiles of Sirtuin family members in the renal tissue of wild-type (WT) mice after inducing hypertensive renal injury by Ang II infusion for 14 days. The relative abundance of each Sirtuin family member was determined by label-free proteomic analysis, and the quantitative expression level of Sirtuin proteins was further verified from a targeted proteomic analysis by Shanghai Applied Protein Technology Co, Ltd[24] (Figure 1A). We found that, among the seven Sirtuin members, SIRT2 showed the most upregulation (Figure 1B), indicating that SIRT2 was the most responsive to hypertensive renal injury.

We then examined renal tissues of 26 patients (13 with and 13 without a history of hypertension), which were obtained from the Department of Urology of the First Hospital of China Medical University. We performed Masson trichrome and alcian blue-periodic acid schiff (AB-PAS) staining to assess the degree of fibrosis and segmental glomerular sclerosis. The renal tissues from the 13 hypertensive patients showed more severe fibrosis and significant glomerulosclerosis compared with the renal tissues from patients without hypertension. Immunohistochemistry staining analysis of SIRT2 expression in samples from the 26 renal tissues showed that SIRT2 expression was significantly higher in the renal tissues of patients with hypertension than in those without a history of hypertension, $P<0.001$ (Figure 1C and 1D). Changes in SIRT2 expression correlated with increased concentration of Ang II in human podocyte cells in vitro. Consistent with previous results, SIRT2 was also highly expressed in Ang II–induced mice (Figure 1E through 1H). Together, these results confirm the involvement of SIRT2 in the hypertensive renal injury response.

We next looked for the specific signal transduction pathway regulated by SIRT2 in the hypertensive renal injury response. Quantitative analysis of the acetylation profiles of hypertensive renal injury tissues from WT, *SIRT2* knockout (*Sirt2*-KO), and Rosa26 (Gt(ROSA)26Sor)-*SIRT2* (silent mating type information regulation 2 homolog-2)-Flag-TG (transgenic) (*SIRT2-TG*) mice were performed (Figure 1I). A total of 11188 acetylation sites and 3470 acetylated proteins were identified by 4-dimensional label-free high-depth proteomics, of which 8284 sites and 2448 proteins showed quantitative differences (Figure S1). Heatmaps (Figure 1J) and volcano plots (Figure 1K, 1L) were used to analyze the differential expression of acetylated proteins in *Sirt2*-KO and *Sirt2*-TG mice compared with the corresponding WT mice. Considered with specific proteomic protein expression analyses (Table S1), the data show

ORIGINAL RESEARCH

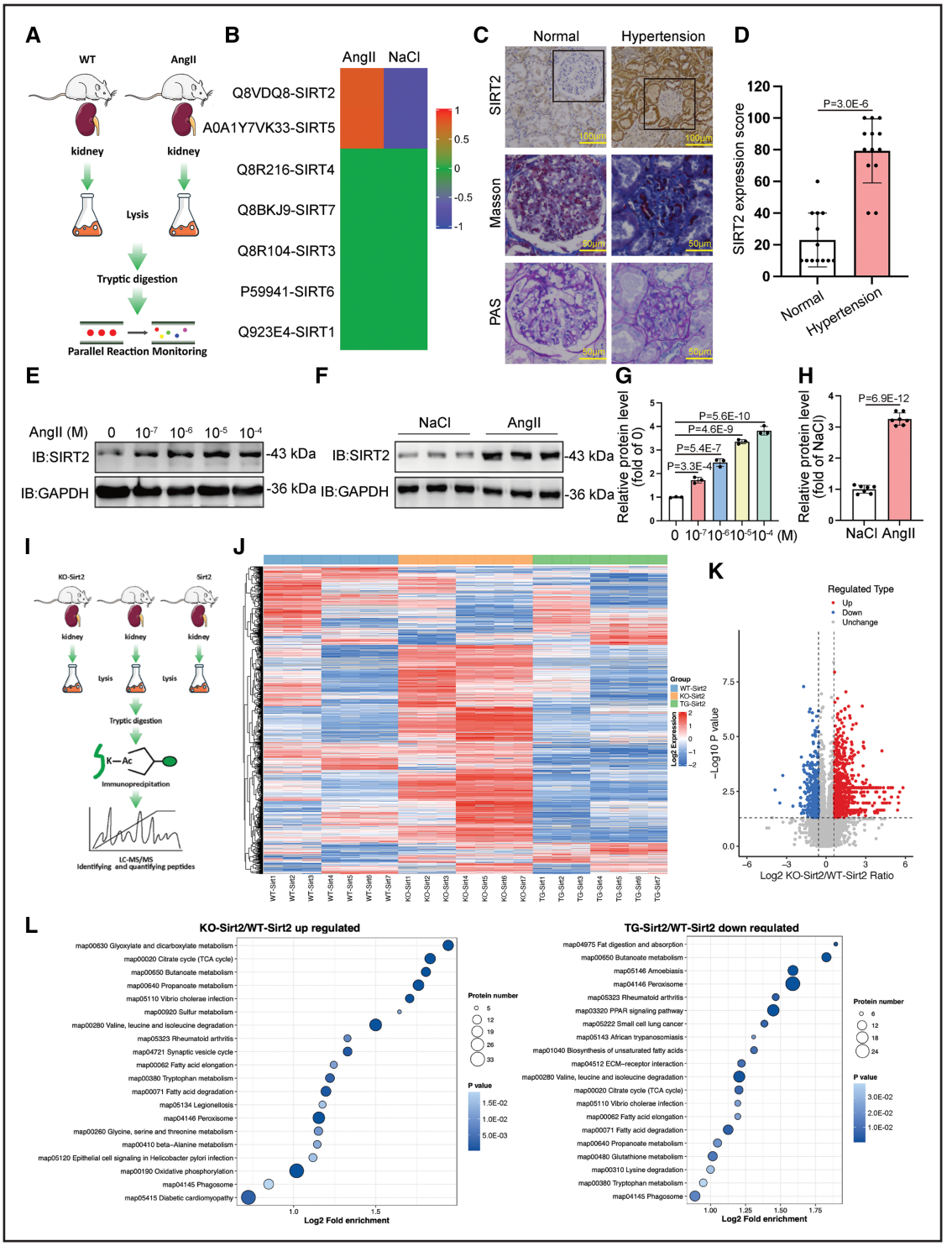

Figure 1. SIRT2 (silent mating type information regulation 2 homolog-2) affects Ang II (angiotensin II)-induced renal podocyte apoptosis through interaction with the GTPase domain of the proapoptosis protein septin4.

A and **B**, Cluster of the Sirtuin protein expression profiles in saline-infused or Ang II–infused mouse kidney tissue at day 14. **C** and **D**, The renal tissues of 26 patients with or without hypertension were stained with Masson trichrome and alcian blue-periodic acid schiff (AB-PAS) to assess the extent of fibrosis and segmental sclerosis and were immunostained with SIRT2 antibody to evaluate SIRT2 expression level (N=26, 13 patients without hypertension, 13 patients with hypertension). SIRT2 stain, scale bar=100 μm; Masson stain and AB-PAS stain, scale bar=50 μm. **E** and **G**, The expression levels of SIRT2 in renal podocyte cells were measured after stimulation with different Ang II concentrations for 48 hours in human podocyte cells. Relative protein levels were calculated as fold changes vs 0 M group (n=3 independent experiments). **F** and **H**, The expression levels of SIRT2 in mice renal tissues were measured after 14 days of Ang II induction. Relative protein levels were calculated as fold changes vs NaCl group, n=7 mice per group. **I**, Workflow showing the quantitative analysis of the acetyl proteomics profiles of hypertensive renal injury tissues in wild-type (WT), *SIRT2* knockout (*Sirt2* KO), and Rosa 26 (Gt(ROSA)26Sor)-*SIRT2* (silent mating type information regulation 2 homolog-2)-Flag-TG (transgenic) (*SIRT2*-TG) mice in kidney samples. **J**, Heatmaps of acetyl protein expression showing the differences (*Continued*)

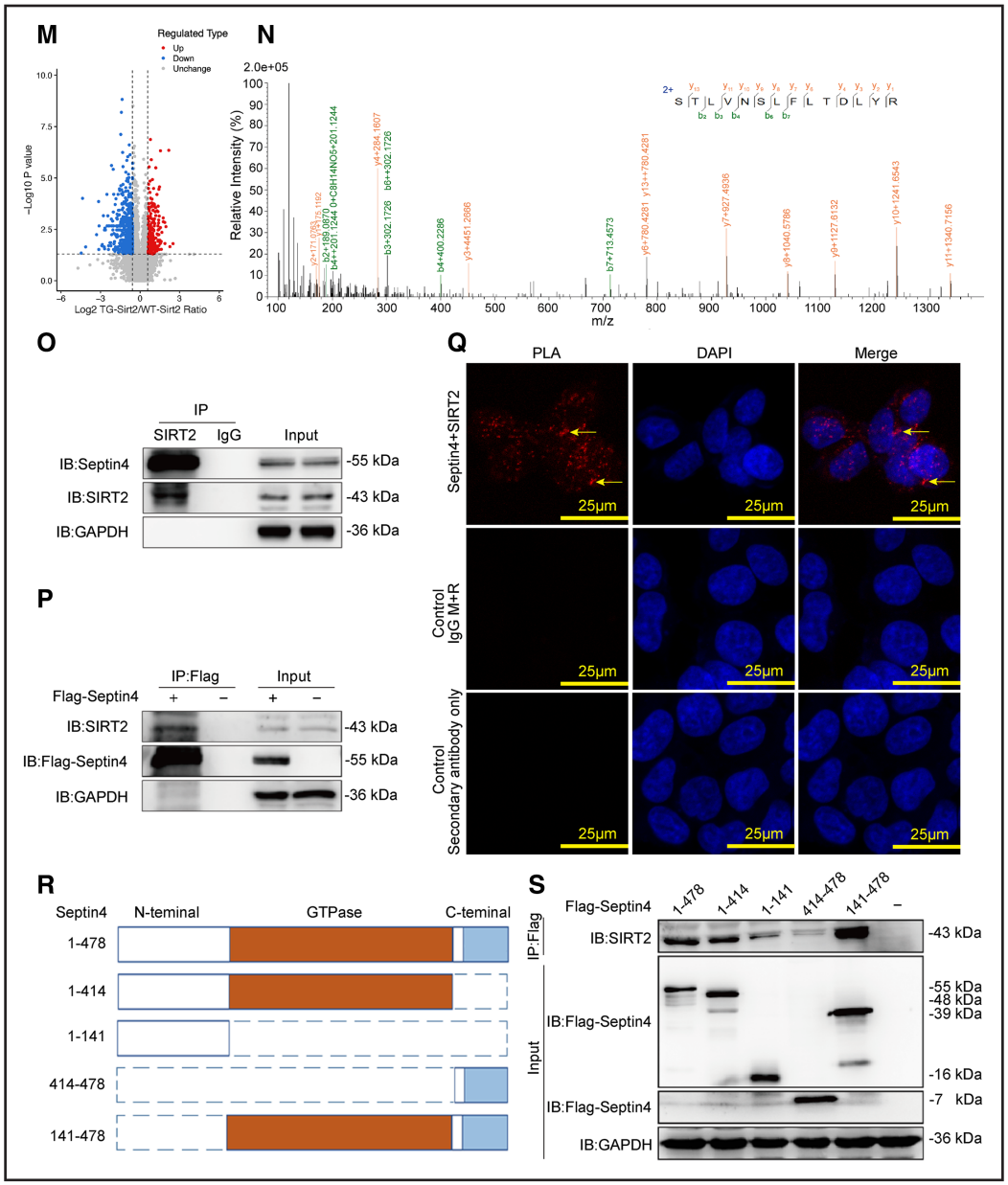

Figure 1. Continued between WT, *Sirt2*-TG, and *Sirt2*-KO mice in hypertensive renal injury tissues. Lines represent individual acetyl protein assays using quantitative mass spectrometry. **K**, Volcano plot showing the fold changes of all detected acetyl proteins and *P* values in the kidneys of mice between the WT and *Sirt2*-KO groups. **L**, Kyoto Encyclopedia of Genes and Genomes (KEGG) pathway enrichment analysis was performed for upregulated expressed acetyl proteins between the WT and *Sirt2*-KO groups, and downregulated expressed acetyl proteins between the WT and *Sirt2*-TG groups in kidney samples. The bubble color reflects Fisher exact test *P* value, the bubble size reflects protein number. **M**, Volcano plot showing the fold changes of all detected acetyl proteins and *P* values in the heart of mice between the WT and *Sirt2*-TG groups. **J**–**M**, n=7 mice per group. **N**, SIRT2 interacting proteins identified by mass spectrometry. **O**, Cell lysates were immunoprecipitated with anti-SIRT2 antibody followed by immunoblotting with antiseptin4 antibody. **P**, Flag-tagged *septin4* plasmid was transfected and total cell lysates were subjected to immunoprecipitation (IP) with anti-Flag antibody followed by detection with SIRT2 antibody. **Q**, Proximity ligation assay (PLA) passes were performed to determine the interaction between SIRT2 and septin4. Red indicates the presence of interaction, and blue (DAPI) indicates nuclear staining. IgG M+R group was used with mouse IgG and rabbit IgG. Scale bar=25 μm. **R**, Septin4 contains three functional domains, including the N-terminal, C-terminal, and GTPase domains. **S**, Full-length or truncated Flag-tagged *septin4* plasmid was transfected. Total cell lysates were subjected to IP with anti-Flag antibody and Western blotting was performed with anti-SIRT2 antibody. Quantitated data were means±SD. The data were not normally distributed for two groups. Statistical significance was assessed by the Mann-Whitney test (**D**). Normality was assumed by the central limit theorem and statistical significance was assessed by 1-way ANOVA with Tukey multiple comparisons test (*P* values adjusted for 10 comparisons; **G**). For data with normality and equal variance, the unpaired *t* test (2-tailed Student *t* test) was used to compare 2 groups (**H**). **J**–**M**, To statistically analyze each proteomics and acetyl proteomics data set, the homoscedastic Student *t* test was used to calculate *P* values for the homoskedasticity data, and the heteroskedastic Student *t* test was used for the heteroskedasticity data. Subsequent screening for differential proteins/sites was based on the *P* value and the ratio of different groups. Differential proteins/sites were displayed using volcano plots and heatmaps (**J**, **K**, **M**). Functional annotation of KEGG enrichment analysis of differential proteins/sites was performed among comparison groups with Fisher exact test. The bubble charts were based on KEGG enrichment significance *P* value (**L**). ECM indicates extracellular matrix; IB, immunoblotting; LC-MS/MS, liquid chromatography-tandem mass spectrometry; and TCA, citrate cycle.

ORIGINAL RESEARCH

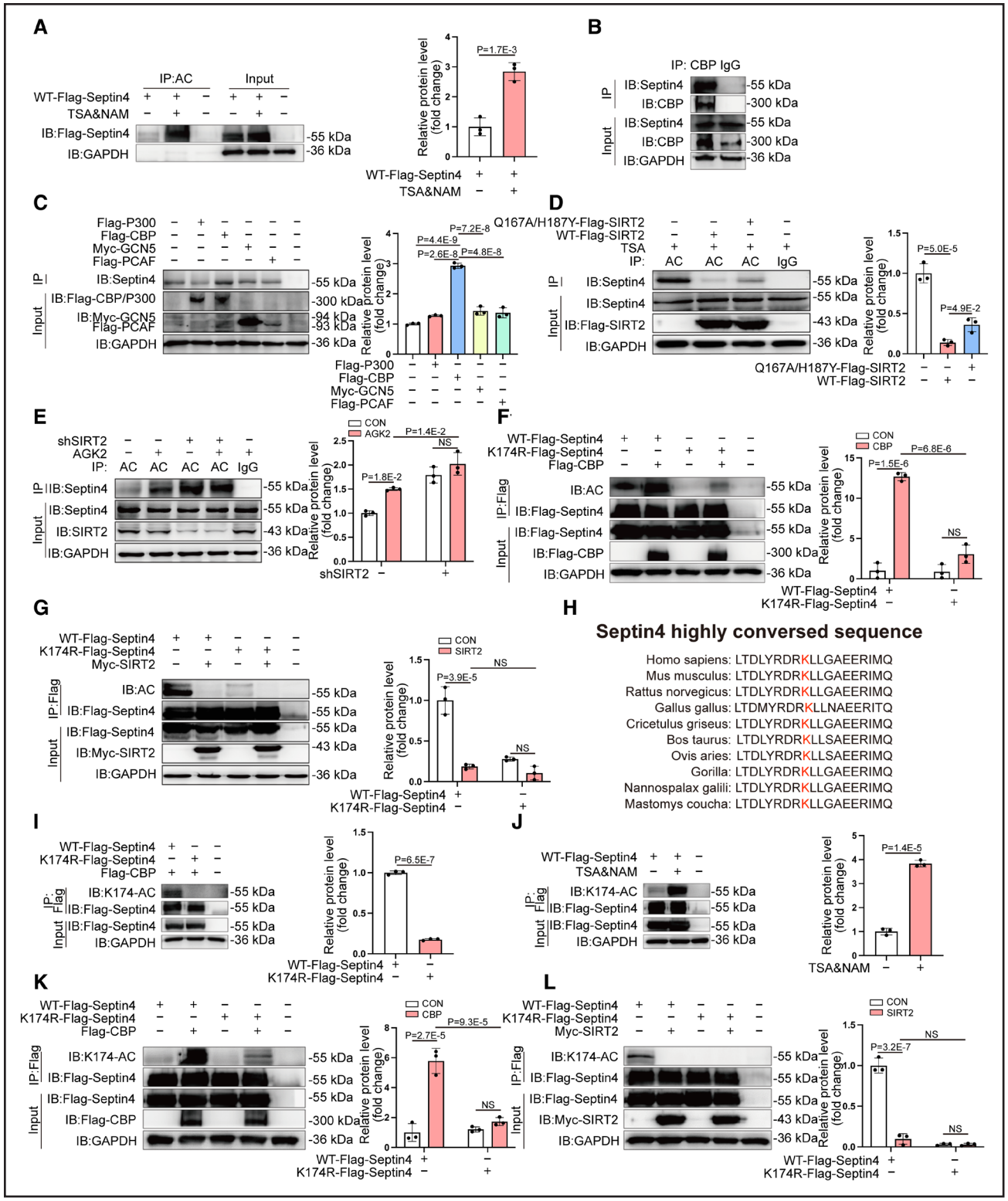

Figure 2. SIRT2 (silent mating type information regulation 2 homolog-2) deacetylates septin4 at lysine 174.
A, Trichostatin A (TSA; 0.5 μM, 16 hours) and nicotinamide (NAM; 5 mM, 4 hours) treated cells were immunoprecipitated with acetylated lysine-specific antibody and detected with antiseptin4 antibody. **B**, Immunoprecipitation of cell lysates showing endogenous septin4 interaction with endogenous CBP (CREB binding protein). **C**, Flag-tagged *CBP, P300* (E1A binding protein), p300/CBP-associated factor (*PCAF* [lysine acetyltransferase 2B]) or Myc-tagged *GCN5* (histone acetyltransferase GCN5) was overexpressed individually, and septin4 was immunoprecipitated with acetylated lysine antibody (Ac-K) and detected with antiseptin4 antibody. **D**, Flag-tagged *SIRT2* wild-type (WT) or H187YQ167A (Mutant) was overexpressed. Septin4 was immunoprecipitated with Ac-K and detected with antiseptin4 antibody. **E**, Normal control and SIRT2 short hairpin RNA (shSIRT2) cells with or without AGK2 ((Z)-2-cyano-3-[5-(2,5-dichlorophenyl)furan-2-yl]-N-quinolin-5-ylprop-2-enamide) (20 μM, 24 hours) (*Continued*)

downregulation of acetylation of most proteins in the *Sirt2*-TG group and upregulation in the *Sirt2*-KO group, indicating that SIRT2 acts as an active deacetylase in hypertensive renal injury. Using the Kyoto Encyclopedia of Genes and Genomes (KEGG) pathway database, we performed functional annotation, enrichment analysis, and visualization of differential acetylation of proteins in the comparison groups (Figure 1M). We found that many pathways that were upregulated in the *Sirt2*-KO group were also downregulated in the *Sirt2*-TG group, including citrate cycle, butanoate metabolism, and peroxisome. These analyses reveal that in the context of hypertensive renal injury, the acetylation level of most proteins involved in basic metabolic regulatory pathways is regulated by SIRT2 and that deacetylation by SIRT2 plays an important role in the response to hypertensive renal injury.

To identify downstream substrates of SIRT2, we performed immunoprecipitation of SIRT2 followed by mass spectrometry analysis. Since hypertension can lead to podocyte apoptosis,[3] we focused on any proteins related to apoptosis. Although a series of subsequent changes eventually lead to glomerulosclerosis,[4–6] the degree of podocyte apoptosis is considered a major prognostic factor for end-stage renal disease.[5] We identified septin4 and PARP1[25] as potential interaction partners of SIRT2 (Table S2, Figure 1N). The interaction between SIRT2 and septin4 was confirmed by coimmunoprecipitation (Figure 1O and 1P), and proximity ligation assay (Figure 1Q). According to the UniProt database, septin4 contains three functional domains, including the N-terminal, C-terminal, and GTPase domains (Figure 1R). Using endogenous SIRT2 and full-length Flag-tagged septin4 or various truncated Flag-septin4 constructs, we found that SIRT2 is bound to the GTPase domain of septin4 (Figure 1S).

Together, these results identify septin4 as a new interaction partner of SIRT2 and indicate that SIRT2 may be involved in Ang II–induced renal podocyte apoptosis via its interaction with the GTPase domain of septin4.

SIRT2 Deacetylates Septin4 at Lysine 174

Given the interaction between SIRT2 and septin4, we asked if the acetylation level of septin4 is modulated through deacetylase activity. Indeed, treatment with trichostatin A and nicotinamide, 2 frequently used deacetylase inhibitors that can repress HDAC (histone deacetylases) I and III[26,27] and the Sirtuin family of deacetylases,[28] resulted in an increase in the acetylation level of septin4 (Figure 2A). To identify the acetyltransferase that acts on septin4, we individually transfected four acetyltransferases, including p300 (E1A binding protein, 300 kDa), CBP (CREB binding protein), PCAF (lysine acetyltransferase 2B; p300/CBP-associated factor), and GCN5 (histone acetyltransferase GCN5). Overexpression of CBP, but not of the other acetyltransferases, markedly enhanced the acetylation level of septin4. Endogenous CBP was confirmed to interact with septin4 (Figure 2B and 2C). Thus, septin4 is a target of the SIRT2 deacetylase and the CBP acetyltransferase.

Next, to further confirm that SIRT2 can deacetylate septin4, we constructed a stable SIRT2 knockdown cell line using three short hairpin RNA (shRNA) fragments. We found that the 22297 fragment produced the best knockdown efficiency (Figure S2F). We compared the acetylation level of septin4 in normal control and SIRT2 short hairpin RNA (shSIRT2) -cells with or without 20 μmol/L AGK2 ((Z)-2-cyano-3-[5-(2,5-dichlorophenyl) furan-2-yl]-N-quinolin-5-ylprop-2-enamide), a commonly used SIRT2-specific inhibitor.[29,30] Consistent with previous results, the acetylation level of septin4 was higher in shSIRT2-cells and in cells treated with AGK2 compared with control cells. Moreover, overexpression of WT-*SIRT2* decreased the acetylation level of endogenous septin4, whereas transfection of a catalytically inactive mutant of *SIRT2* (H187YQ167A) had no effect (Figure 2D and 2E).

We then set out to identify the site on septin4 that is deacetylated by SIRT2. We examined proteomic profiling data in the PhosphoSitePlus PTM database (Cell Signaling Technology) and identified K174 as a

Figure 2 Continued. treatment were immunoprecipitated with antiacetylation lysine antibody and detected with antiseptin4 antibody. **F**, Flag-tagged *CBP* was cotransfected with Flag-tagged *septin4* WT or K174R (Mutant). Septin4 acetylation was detected by immunoprecipitation (IP) using Ac-K. **G**, Myc-tagged *SIRT2* was cotransfected with Flag-tagged *septin4* WT or K174R (Mutant). Septin4 acetylation was detected using Ac-K. **H**, Alignment of sequences surrounding K174 in septin4 homologs from diverse species. Acetylated lysine residues at septin4-K174 are highlighted (bold and red). **I**, Flag-*septin4* or Flag-K174R-*septin4* plasmid was introduced into cells by transfection, and total lysates were immunoprecipitated with anti-Flag antibodies, followed by immunoblot with acetyl-K174 site-specific antibody. **J**, The Flag-*septin4* plasmid was transfected into 293T cells treated with NAM (5 mM, 4 hours) and TSA (0.5 μM, 16 hours), followed by immunoprecipitation with anti-Flag antibodies. K174-Acetylation of exogenous septin4 was analyzed by immunoblot with acetyl-K174 site-specific antibody. **K**, The Flag-*septin4* plasmid or the Flag-K174R-*septin4* plasmid was cotransfected with Flag-control or Flag-*CBP* plasmid into 293T cells, followed by immunoprecipitation with anti-Flag antibodies. K174-Acetylation of exogenous septin4 was analyzed by immunoblot with acetyl-K174 site-specific antibody. **L**, The Flag-*septin4* plasmid or the Flag-K174R-*septin4* plasmid was cotransfected with Myc-control or Myc-*SIRT2* plasmid into 293T cells, followed by immunoprecipitation with anti-Flag antibodies. K174-Acetylation of exogenous septin4 was analyzed by immunoblot with acetyl-K174 site-specific antibody. Three independent experiments were performed. Based on the central limit theorem the data were considered to be normally distributed. Relative protein levels were calculated as fold changes vs the first group. **A**–**L**, Quantitated data were means±SD. Statistical significance was assessed by unpaired *t* test (2-tailed Student *t* test; **A**, **I** and **J**); 1-way ANOVA with Tukey multiple comparisons test (**C**, *P* values adjusted for 10 comparisons; **D**, *P* values adjusted for 3 comparisons); 2-way ANOVA with Bonferroni multiple comparisons test (**E**–**G**, **K**–**L**, *P* values adjusted for 6 comparisons). AC indicates acetylated antibody; CON, control group, without treatment; IB, immunoblotting; and NS, not statistically significant.

ORIGINAL RESEARCH

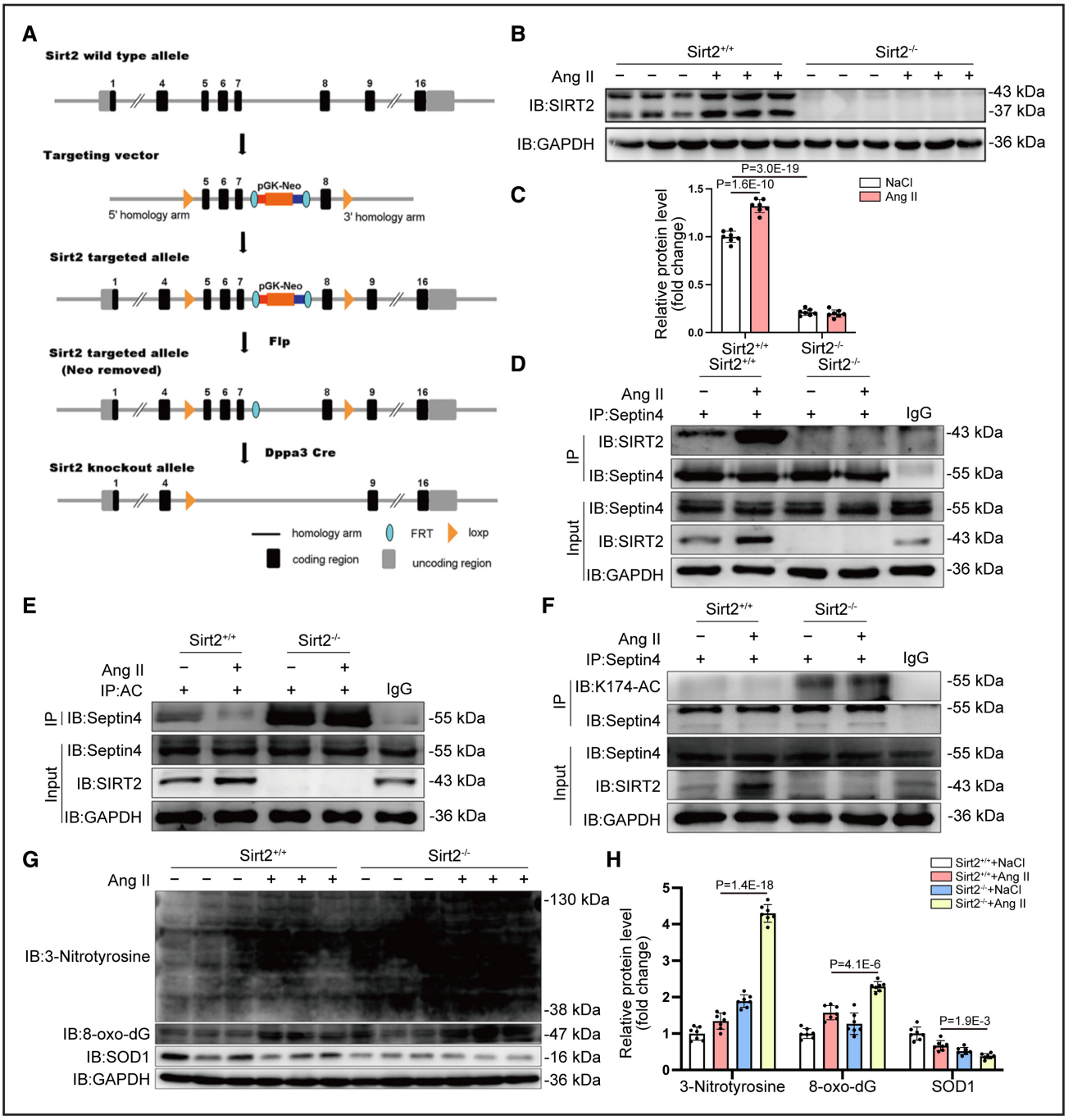

Figure 3. Sirt2 (silent mating type information regulation 2 homolog-2)-knockout mice show increased acetylation of septin4 and significant aggravation of Ang II (angiotensin II)–induced hypertensive renal injury.

A, Diagram showing the method of construction of the *Sirt2* knockout mice. **A**–**V**, Total protein was obtained from *Sirt2*–wild-type (WT) and *Sirt2*$^{-/-}$ mice renal tissue after Ang II (1.5 mg/kg per day) infusion for 14 days. **B** and **C**, Western blot was carried out to assess SIRT2 expression levels. **D**, Total lysates of renal tissue were subjected to immunoprecipitation (IP) with antiseptin4 antibody and Western blot with anti-SIRT2 antibody. **E**, Total lysates of renal tissue were subjected to IP with pan acetylation antibody (AC) and Western blot with antiseptin4 antibody in *SIRT2* knockout (*Sirt2*-KO) mice. **F**, Total lysates of renal tissue were subjected to IP with antiseptin4 antibody and Western blot with K174-AC (acetyl-K174 site-specific antibody) in *Sirt2*-KO mice. **G** and **H**, Western blot was carried out to assess expression levels of 3-nitrotyrosine, 8-oxo-2'-deoxyguanosine (8-oxo-dG), and SOD1(Superoxide Dismutase 1). **I** and **J**, Renal tissues were stained using the DCFH-DA (2,7-Dichlorodihydrofluorescein diacetate) Assay Kit (red). Scale bar=100 μm. **K** and **L**, Western blot was carried out to assess precursors of PARP1 (poly [ADP-ribose] polymerase family, member 1) and caspase3, cleaved-PARP1, and cleaved-caspase3 expression levels. **M** and **N**, Renal function was evaluated by (**M**) hour urinary protein creatinine ratio (UPCR) and (**N**) creatinine clearance (ml/min). **O** and **S**, Hematoxylin and eosin (H&E) staining was carried out to assess degree of glomerular edema. Arrowheads, renal tubular edema. Scale bar=50 μm. **P** and **T**, AZAN (azocarmine G and anline blue) trichrome staining was carried out to assess content of extracellular matrix secretion in glomeruli. Arrowheads, extracellular matrix of glomerulus (blue). Scale bar=20 μm. **Q** and **U**, AB-PAS (alcian blue-periodic acid schiff) staining was carried out to assess glomerular sclerosis. Arrowheads, segmental sclerosis of glomerulus (lilac color). Scale bar=20 μm. **R** and **V**, (*Continued*)

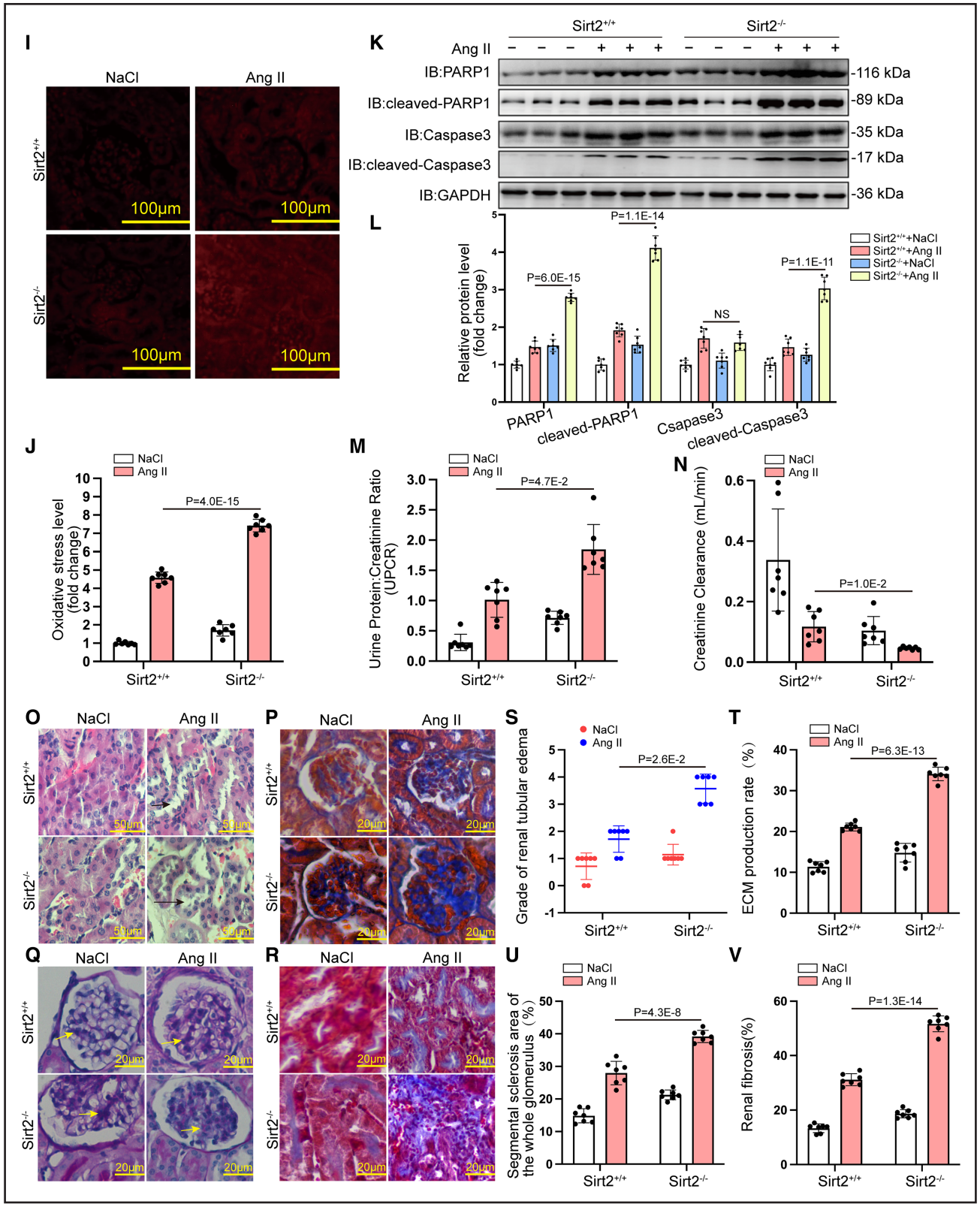

Figure 3. Continued Masson staining was carried out to assess the degree of glomerular fibrosis. Arrowheads, glomerular fibrosis (blue). Scale bar=20 μm. **B**, **C**, **G**–**V**, For data with normality and equal variance, 2-way ANOVA with Bonferroni test was used to compare groups. If normality or homogeneity of variance was not met, treatment differences were assessed by Kruskal-Wallis test with Dunn multiple comparisons test (n=7 mice per group). Relative protein levels were calculated as fold changes vs the first group. Quantitated data are means±SD. Statistical significance was assessed by 2-way ANOVA with Bonferroni multiple comparisons test (**C**, **H**, **J**, **L**, **T**–**V**, *P* values adjusted for 6 comparisons); Kruskal-Wallis with Dunn multiple comparisons test (**M**, **N**, **S**, *P* values adjusted for 1 comparisons). DPPA3 indicates, developmental pluripotency associated 3; FLP, flippase; FRT, flippase recognition target; IB, immunoblotting; NS, not statistically significant; and pGK-neo, phosphoglycerate kinase-neo.

potential acetylation site. We mutated the lysine (K) 174 acetylation site to arginine (R, nonacetylatable mutant) using site-directed mutagenesis. Cells were transfected with plasmids expressing WT-*septin4* or the *Septin4*-K174R mutant simultaneously with the Flag-control or Flag-*CBP* plasmid. *Septin4*-K174R showed a diminished level of acetylation regardless of the presence of CBP, whereas the level of acetylation of WT-septin4 increased with coexpression of CBP (Figure 2F). Similarly, Septin4-K174R was unaffected with or without SIRT2 overexpression, in contrast to WT-septin4 (Figure 2G). Together, our findings identify CBP as the acetyltransferase of septin4, which is also a target for SIRT2-dependent deacetylation. K174 is evolutionarily conserved from *Gallus* to mammals (Figure 2H) and is likely the major acetylation site in septin4 that is regulated by SIRT2.

To further investigate the functional role of K174 acetylation, we generated an antibody that specifically recognizes ectopically expressed WT, but not septin4-K174R (Figure 2I). Treatment with trichostatin A and nicotinamide resulted in an increase in the acetylation level of septin4-K174 (Figure 2J). Septin4-K174R acetylation level was unaffected with or without CBP overexpression, whereas the WT-septin4 acetylation level increased with CBP overexpression (Figure 2K). Septin4-K147R was also unaffected with or without SIRT2 overexpression as compared with WT-septin4 (Figure 2L). These results indicate that CBP can acetylate the Septin-K174 site and that SIRT2 deacetylates this site.

Sirt2-Knockout Mice Show Increased Acetylation of Septin4 and Significant Aggravation of Ang II–Induced Hypertensive Renal Injury

To establish the role of SIRT2-septin4 signal transduction in hypertensive renal injury, we first confirmed that Ang II induction leads to increased binding between SIRT2 and septin4 in renal podocytes (Figure S3A). Furthermore, the acetylation level of septin4 was decreased with Ang II, while it was increased in shSIRT2-treated renal podocytes. The acetylation level of septin4 was normalized after reexpression of WT-*SIRT2*-NTm (a shRNA nontargetable mutant SIRT2 rescue plasmid) in shSIRT2 renal podocytes (Figure S3B).

We then focused on the role of SIRT2 in hypertensive renal injury and established an in vivo hypertensive renal injury model in *Sirt2*-WT and *Sirt2*$^{-/-}$ C57BL/6 mice by infusing Ang II for 2 weeks via osmotic minipumps. Deletion of *SIRT2* exons 5-8 in *Sirt2* knockout mice (Figure 3A) was confirmed by Western blotting (Figure 3B and 3C).[31] Although the blood pressure of *Sirt2*-WT and *Sirt2*$^{-/-}$ mice increased significantly with induction by Ang II ($P<0.001$), there was no significant difference in the blood pressure between *Sirt2*-WT and *Sirt2*$^{-/-}$ mice (Figure S2J). Consistent with our results in podocytes, the interaction between SIRT2 and septin4 increased (Figure 3D), whereas the acetylation level of septin4 decreased (Figure 3E) in the hypertensive renal injury mice. By contrast, the septin4 acetylation level was elevated in *Sirt2* knockout mice (Figure 3E). Furthermore, consistent with previous results, immunoprecipitation assays using the acetyl-K174 site-specific antibody showed that the acetylation level of septin4-K174 increased in the hypertensive renal injury tissues of *Sirt2* knockout mice (Figure 3F).

Hypertension causes progressive damage in the kidney. Kidney volume and swelling of tubular epithelial cells increase and glomerular mesangial matrix deposition also increase in the early stage.[32,33] Whereas *Sirt2*$^{-/-}$ mice lacked *Sirt2*, kidney tissue from *Sirt2*-WT mice showed a significant increase in the expression of SIRT2 after hypertensive injury induced by Ang II (Figure 3B and 3C). Simultaneous staining of several oxidative stress–related markers including 3-nitrotyrosine, 8-oxo-2'-deoxyguanosine (8-oxo-dG), and SOD1(Superoxide Dismutase 1), as well as measurement of the endogenous oxidative stress level, were performed on the renal tissues from WT and *Sirt2*$^{-/-}$ knockout mice. Higher oxidative stress–related proteins (Figure 3G and 3H) and oxidative stress level (Figure 3I and 3J) were observed in *Sirt2*$^{-/-}$ mice compared with WT.

To determine if hypertensive renal injury was accompanied by changes in the expression of apoptosis-related proteins, we compared *Sirt2*-WT and *Sirt2*$^{-/-}$ groups and found that *Sirt2*$^{-/-}$ showed a markedly elevated abundance of cleaved-PARP1 and cleaved-caspase3 (Figure 3K and 3L). We also analyzed the precursor levels of PARP1 and caspase3. The level of PARP1 increased significantly after the induction of Ang II, particularly in *Sirt2*$^{-/-}$ groups compared with *Sirt2*-WT groups. This is caused by a decrease in PARP1 ubiquitination mediated by the proteasome after *Sirt2* knockout, which is consistent with our previous research.[25] The caspase3 precursor also increased after Ang II induction, in line with previous research,[34] but the level of caspase3 was not affected by SIRT2.

Our results above show that *Sirt2* knockout mice display aggravated oxidative stress injury and apoptosis in hypertensive renal injury. Proteinuria is the clinical signature of podocyte apoptosis and may occur with or without loss of renal function due to glomerulosclerosis.[5] Proteinuria is both a marker of hypertensive renal complications and a major risk factor for the progression to end-stage renal disease.[4] To explore the level of proteinuria and the degree of renal function damage, 24-hour urine samples were collected from mice after 2 weeks of Ang II–induced hypertensive renal injury. The 24-hour urinary protein creatinine ratio (UPCR) of *Sirt2*$^{-/-}$ mice was significantly higher than that of WT mice (Figure 3M), while the Creatinine Clearance (mL/min) of the *Sirt2* knockout

was significantly lower (Figure 3N). Thus, *Sirt2* knockout mice displayed deteriorating renal function in hypertensive renal injury.

We next assessed the role of SIRT2 in tubular epithelial cell edema and excessive glomerular mesangial matrix formation using hematoxylin and eosin (H&E) staining and AZAN (azocarmine G and anline blue) trichrome staining in the early stage of hypertensive injury. Concurrently, we assessed the role of SIRT2 in glomerulosclerosis and renal fibrosis via AB-PAS (alcian blue-periodic acid schiff) and Masson staining in the late stage of renal injury. As expected, H&E, Azan trichrome (Figure 3O, 3P, 3S, and 3T) AB-PAS, and Masson staining (Figure 3Q, 3R, 3U, and 3V) all showed that *Sirt2* knockout significantly aggravated early and advanced hypertensive renal injury.

Gradient analysis revealed that the levels of the apoptosis factors cleaved-caspase3 and cleaved-PARP1 were highest at 10^{-5} mol/L Ang II. At this Ang II concentration cell viability decreased, the cytoskeleton disintegrated, and noncell necrosis occurred. Therefore, 10^{-5} mol/L Ang II was determined to be the optimal concentration for significant induction of renal podocyte apoptosis (Figure S2A through S2E). We then tested normal control and shSIRT2-renal podocytes with or without 10^{-5} mol/L Ang II–induced oxidative stress injury of renal podocytes. The shSIRT2 cells showed increased levels of 3-nitrotyrosine, 8-oxo-dG, SOD1, and intracellular oxidative stress levels in response to oxidative stress injury, while transient reexpression of WT-*SIRT2* NTm in SIRT2-depleted renal podocytes rescued the injury (Figure S3C through S3F). Similarly, shSIRT2 cells showed an increased level of cleaved-PARP1 (Figure S3G through S3H) and severe disintegration of the cytoskeleton (Figure S3J and S3K) in response to renal podocyte injury, while transient reexpression of WT-*SIRT2* NTm in SIRT2-depleted renal podocytes rescued the apoptosis. Similar results were obtained using the CCK8 (Cell Counting Kit-8) assay (Figure S3I). In the same way, the level of PARP1 in shSIRT2 cells was higher than that in the normal control group, while the level of PARP1 recovered after reexpression of WT-*SIRT2* NTm in SIRT2-depleted renal podocytes (Figure S3G). Combined, these results demonstrate a high acetylation level of septin4 and significantly aggravated Ang II–induced hypertensive renal injury in *Sirt2*-knockout mice.

SIRT2 Overexpression Results in Decreased Acetylation of Septin4 and Significant Reduction of Ang II–Induced Hypertensive Renal Injury

To further explore the role of SIRT2 in hypertensive renal injury, we constructed Rosa26-*Sirt2*-Flag (*Sirt2*-TG) mice (Figure 4A) by mating F0 generation mice with *Dppa3* cre mice. The resulting *SIRT2*-TG mice were confirmed by Western blotting (Figure 4B). To detect the subcellular distribution of overexpressed Sirt2 in transgenic mice, we separated the cytoplasm, nucleus, and mitochondria in kidney tissue from *Sirt2*-TG mice and analyzed them by immunoblotting. *Sirt2*-TG mice showed increased Sirt2 not only in the cytoplasm but also in the nuclei and mitochondrial fractions. The overexpressed Flag-SIRT2 was largely in the cytoplasm, with less accumulation in the nucleus and mitochondria (Figure 4C and 4D), consistent with previous studies of the subcellular distribution of SIRT2.[35,36]

Whereas the blood pressure of both *Sirt2*-WT and *Sirt2*-TG mice increased significantly upon induction by Ang II ($P<0.001$), there was no significant difference in the blood pressure between *Sirt2*-WT and *Sirt2*-TG mice (Figure S2K). The acetylation level of septin4 in *Sirt2*-TG was decreased (Figure 4E). Moreover, consistent with previous results, immunoprecipitation using the acetyl-K174 site-specific antibody showed that the acetylation level of septin4-K174 was decreased in hypertensive renal injury tissues of *Sirt2*-TG mice (Figure 4F).

Our findings indicated that SIRT2 modulates septin4 through deacetylation of K174. Several Ang II–induced oxidative stress injury markers were detected, including 3-Nitrotyrosine, 8-oxo-dG, and SOD1, and endogenous oxidative stress levels were measured in renal tissues of WT and *Sirt2*-TG mice. The expression of oxidative stress–related proteins (Figure 4G and 4H) and the endogenous oxidative stress levels (Figure 4I and 4J) decreased significantly with SIRT2 overexpression compared with WT, indicating that the level of oxidative stress was decreased in *Sirt2*-TG mice. In addition, compared with the WT group, the *Sirt2*-TG group had markedly reduced amounts of cleaved-PARP1 and cleaved-caspase3 (Figure 4K and 4L). Moreover, the precursor levels of PARP1 and caspase3 increased with the induction of Ang II. The level of PARP1 decreased in *Sirt2*-TG groups compared with *Sirt2*-WT groups, consistent with our previous research,[25] while the precursor of caspase3 showed no significant difference between the 2 groups. Thus, *Sirt2*-TG mice displayed less oxidative stress injury and apoptosis in hypertensive renal injury. Consistently, UPCR of *Sirt2*-TG mice was significantly lower than that of WT mice (Figure 4M), whereas the creatinine clearance (mL/min) of *Sirt2*-TG mice was significantly higher (Figure 4N), indicating that *Sirt2*-TG mice displayed improved renal function in hypertensive renal injury.

Sirt2-TG mice showed significant reduction in the degree of renal tubular edema and a decrease in the area of the glomerular mesangial matrix after Ang II–induced injury compared with WT mice (Figure 4O, 4P, 4S, 4T). AB-PAS and Masson staining indicated

ORIGINAL RESEARCH

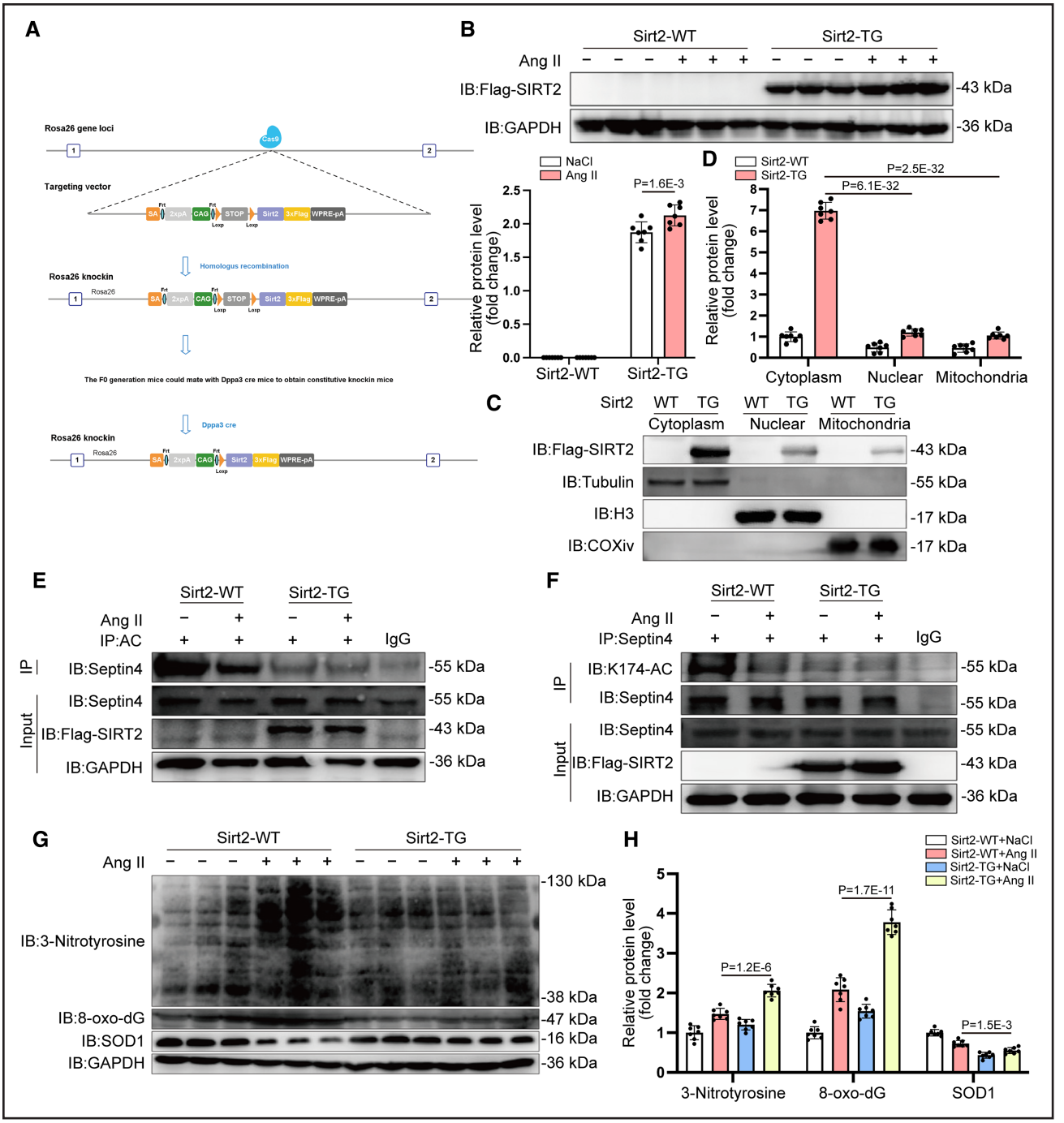

Figure 4. SIRT2 (silent mating type information regulation 2 homolog-2) overexpression results in decreased acetylation of septin4 and significant reduction of Ang II (angiotensin II)–induced hypertensive renal injury.

A, Diagram showing the method of construction of Rosa 26 (Gt(ROSA)26Sor)-*SIRT2* (silent mating type information regulation 2 homolog-2)-Flag-TG (transgenic) (*SIRT2*-TG) mice. **B**, Total protein was obtained from wild-type (WT) and *Sirt2*-TG mice renal tissue after Ang II (1.5 mg/kg per day) infusion for 14 days. Western blot was carried out to assess Flag-tagged SIRT2 expression levels. **C** and **D**, Cytoplasm, nucleus, and mitochondria of kidney tissue from *Sirt2*-TG mice were isolated. Western blotting was carried out to assess Flag-tagged SIRT2 expression levels in the 3 fractions. **E**, Total lysates of renal tissue from *Sirt2*-TG mice were subjected to immunoprecipitation (IP) with antiacetylation antibody (AC) and Western blot with antiseptin4 antibody. **F**, Total lysates of renal tissue from *Sirt2*-TG mice were subjected to IP with antiseptin4 antibody and Western blot with anti–K174-acetylation specific antibody (K174-AC). **G** and **H**, Western blot was carried out to assess 3-nitrotyrosine, 8-oxo-2'-deoxyguanosine (8-oxo-dG) and SOD1 (Superoxide Dismutase 1) expression levels. **I** and **J**, Renal tissues were stained using DCFH-DA (2,7-Dichlorodihydrofluorescein diacetate) Assay Kit (red). Scale bar=100 μm. **K** and **L**, Western blot was carried out to assess precursors of PARP1 (poly [ADP-ribose] polymerase family, member 1) and caspase3, cleaved-PARP1, and cleaved-caspase3 expression levels. **M** and **N**, Renal function was evaluated by (**M**) hour urinary protein creatinine ratio (UPCR) and (**N**) Creatinine Clearance (mL/min). **O** and **S**, Hematoxylin and eosin (H&E) staining was carried out to assess the degree of glomerular edema. Arrowheads, renal tubular edema. Scale bar=50 μm. **P** and **T**, AZAN (azocarmine G and anline blue) trichrome staining was carried out to assess the content of extracellular matrix secretion in glomeruli. Arrowheads, extracellular matrix of glomerulus (blue). Scale bar=20 μm. (*Continued*)

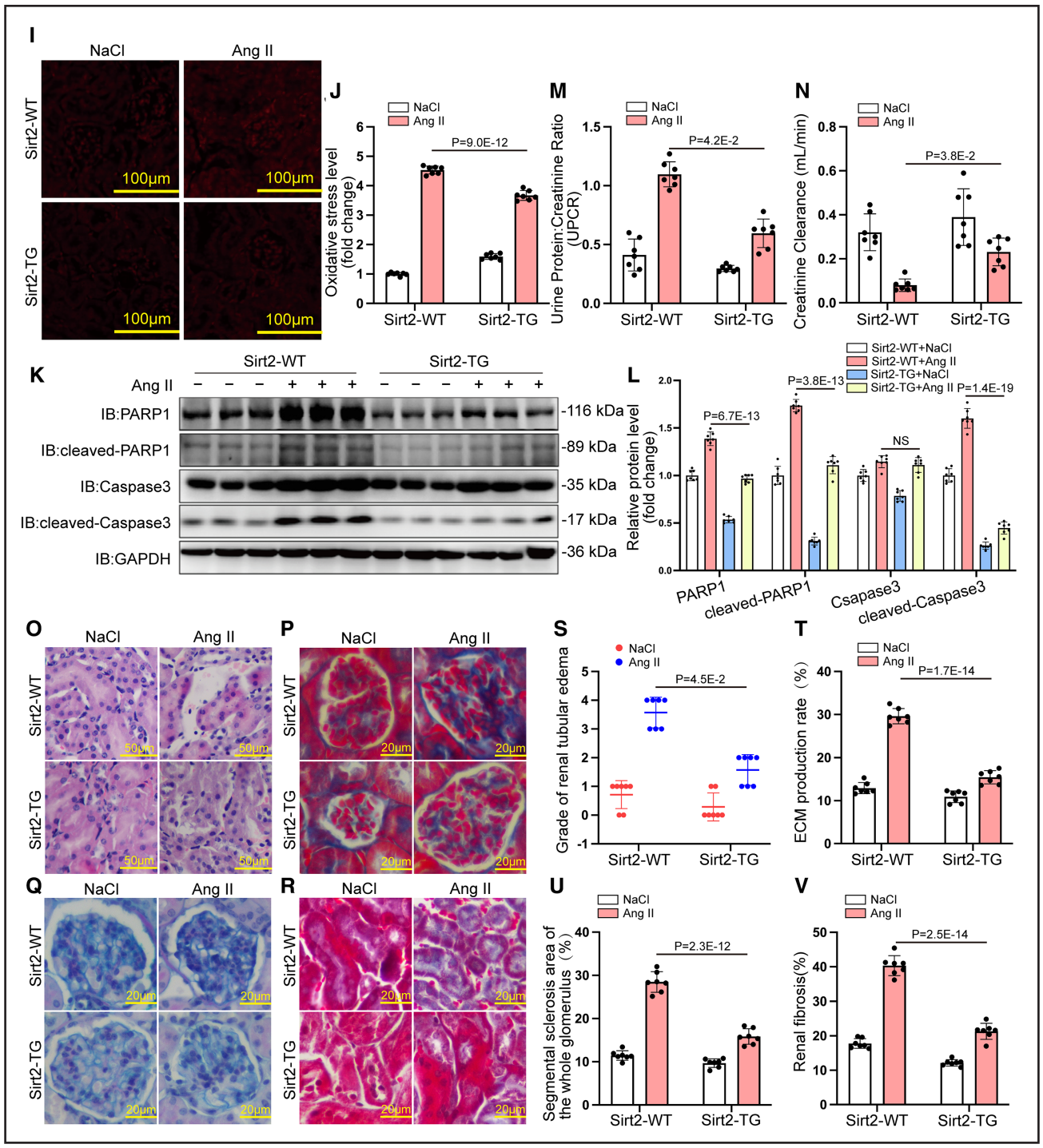

Figure 4. Continued **Q** and **U**, AB-PAS (alcian blue-periodic acid schiff) staining was carried out to assess glomerular sclerosis. Arrowheads, segmental sclerosis of glomerulus (lilac color). Scale bar=20 μm. **R** and **V**, Masson staining was carried out to assess the degree of glomerular fibrosis. Arrowheads, glomerular fibrosis (blue). Scale bar=20 μm. **B**–**D**, **G**–**V**, For data with normality and equal variance, 2-way ANOVA with Bonferroni test was used to compare groups. If normality or homogeneity of variance was not met, treatment differences were assessed by Kruskal-Wallis test with Dunn multiple comparisons test (n=7 mice per group). Relative protein levels were calculated as fold changes vs the first group. Quantitated data are means±SD. Statistical significance was assessed by 2-way ANOVA with Bonferroni multiple comparisons test (**B**, **H**, **J**, **L**, **T**–**V**, *P* values adjusted for 6 comparisons; **D**, *P* values adjusted for 15 comparisons); Kruskal-Wallis with Dunn multiple comparisons test (**M**, **N**, **S**, *P* values adjusted for 1 comparisons. COXiv indicates cytochrome c oxidase subunit IV; IB, immunoblotting; and NS, not statistically significant.

that both the segmental sclerosis and fibrosis area in *Sirt2*-TG mice were smaller than those in WT mice after hypertensive renal injury ($P<0.001$; Figure 4Q, 4R, 4U, and 4V). Therefore, *Sirt2*-TG mice showed mitigated Ang II–induced hypertensive renal injury. These results further underscore the finding that deacetylated

ORIGINAL RESEARCH

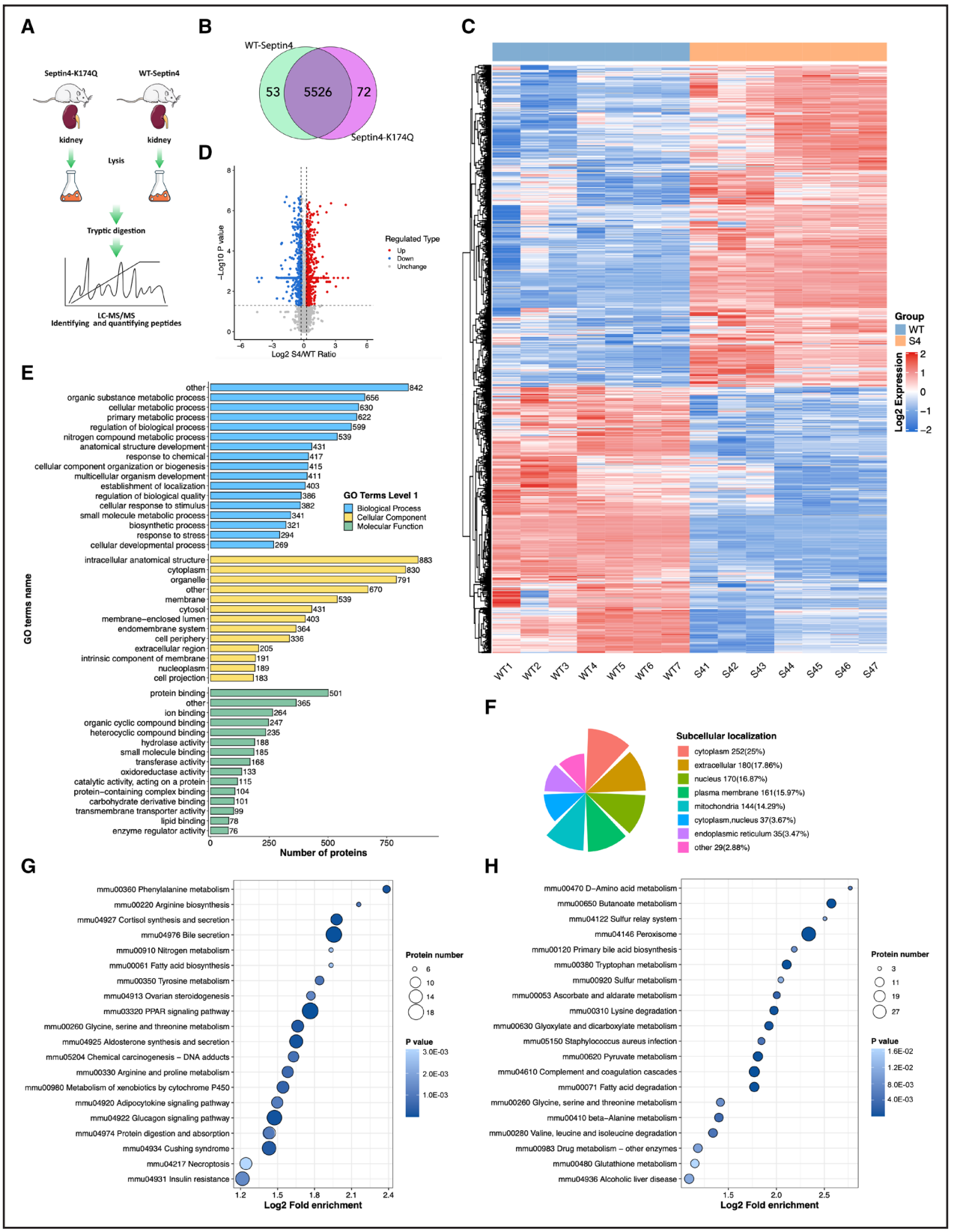

Figure 5. Septin4-K174Q proteomic analysis suggests a role for septin4 in the peroxisome and apoptosis pathways. **A**, Workflow chart showing the quantitative analysis of the proteome profiles of kidney samples from *septin4* K174Q and wild-type (WT) animals (n=7 per mice group). **B**, Venn diagram showing identified proteins in mouse kidney tissues that overlap between the *septin4*-K174Q and WT-*septin4* groups. **C**, Heatmaps of protein expression levels in kidney samples showing differences between *septin4*-K174Q and WT-*septin4* mice. Lines represent individual protein assays by quantitative mass spectrometry. **D**, Volcano plot showing the fold changes of all (*Continued*)

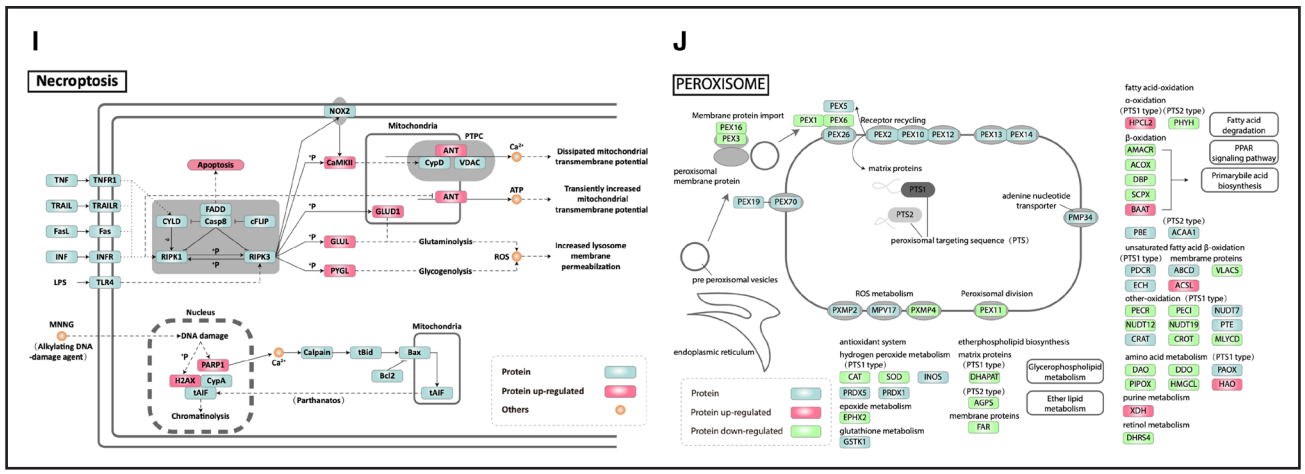

Figure 5. Continued detected proteins and *P* values in the heart of mice between the *septin4*-K174Q and WT-*septin4* groups. **E**, Gene Ontology (GO) classification showing differentially expressed proteins in kidney samples between *septin4*-K174Q and WT-*septin4* mice. Bar length represent protein number. **F**, Differentially expressed proteins in the kidney of *septin4*-K174Q and WT-*septin4* mice were predicted and classified for subcellular structural mapping. **G** and **H**, Kyoto Encyclopedia of Genes and Genomes (KEGG) pathways enrichment analysis in the kidney was performed for upregulated (**G**) and downregulated (**H**) expressed proteins between the WT-*septin4* and *septin4*-K174Q groups. The bubble color reflects Fisher exact test *P* value, the bubble size reflects protein number. **I**, Necroptosis pathway showing the distribution of differentially expressed proteins. **J**, Peroxisome pathway showing the distribution of differentially expressed proteins. S4 represents *septin4*-K174Q mice. To statistically analyze each proteomics and acetyl proteomics data set, the homoscedastic Student *t* test was used to calculate *P* values for the homoskedasticity data, and the heteroskedastic Student *t* test was for the heteroskedasticity data. Subsequent screening for differential proteins/sites was based on the *P* value and the ratio of different groups. Differential proteins/sites were displayed using volcano plots and heatmaps (**C** and **D**). Functional annotation of GO and Subcellular Localization of differential proteins/sites were shown among comparison groups (**E** and **F**). Functional annotation of KEGG enrichment analysis of differential proteins/sites were performed among comparison groups with Fisher exact test. The bubble charts were based on KEGG enrichment significance *P* value (**G** and **H**). PPAR indicates poly (ADP-ribose) polymerase family, member 1. LC-MS/MS indicates liquid chromatography-tandem mass spectrometry.

septin4-dependent regulation by SIRT2 alleviates hypertensive renal injury.

To determine the exact role of deacetylation of septin4 via SIRT2 in hypertensive renal injury, we constructed stable septin4 knockdown (shSeptin4) renal podocytes using three shRNA fragments (Figure S2H). The knockdown efficiency of the 72650 fragment was highest and was used for experiments. We analyzed normal control and shSeptin4-renal podocytes with or without 10^{-5} mol/L Ang II–induced oxidative stress injury of renal podocytes. After reexpression of WT-*septin4* NTm, the level of oxidative stress was higher than in shSeptin4, while there was no obvious change after reexpression of K174R NTm in septin4-depleted renal podocytes, compared with shSeptin4 (Figure S4A through S4D). The level of cleaved-PARP1 and cleaved-caspase3 after reexpression of WT-*septin4* NTm was higher than in shSeptin4, while there was no significant difference between transient reexpression of K174R NTm in septin4-depleted or shSeptin4 renal podocytes (Figure S4E and S4F). Similar results were obtained using CCK8 assays (Figure S4J). The precursors of PARP1 and caspase3 were detected, but there was no significant difference among the three groups with or without Ang II (Figure S4E and S4F). In addition, the level of cleaved-caspase8 and cleaved-caspase9 after reexpression of WT-*septin4* NTm was also higher than in shSeptin4, whereas there was no significant difference with transient reexpression of K174R NTm in septin4-depleted or shSeptin4 renal podocytes (Figure S4G and S4H). The increase in cleavage of caspase8 and caspase9 indicates activation of the extrinsic and intrinsic pathways of apoptosis.[37] Septin4 is an important component of the cytoskeleton and can act as a scaffold for protein recruitment.[38] We therefore also examined the degree of cytoskeleton disintegration after reexpression of WT-*septin4* NTm and found it was higher than in shSeptin4, whereas there was no significant difference between transient reexpression of K174R NTm in septin4-depleted or shSeptin4 renal podocytes (Figure S4I and S4K).

Together, our results show that SIRT2 relieved Ang II–induced renal podocyte apoptosis by deacetylation of K174 of septin4 via activation of extrinsic and intrinsic pathways of apoptosis.

Septin4-K174Q Proteomic Analysis Suggests a Role for Septin4 in the Peroxisome and Apoptosis Pathways

To explore the role of septin4-K174 acetylation in hypertensive renal injury, we constructed *septin4*-K174Q mutant mice (acetylation mimic), in which lysine 174 (AAA) of F1 generation mice is mutated to glutamine (CAA; Figure 6A). We validated the *septin4*-K174Q transgenic

ORIGINAL RESEARCH

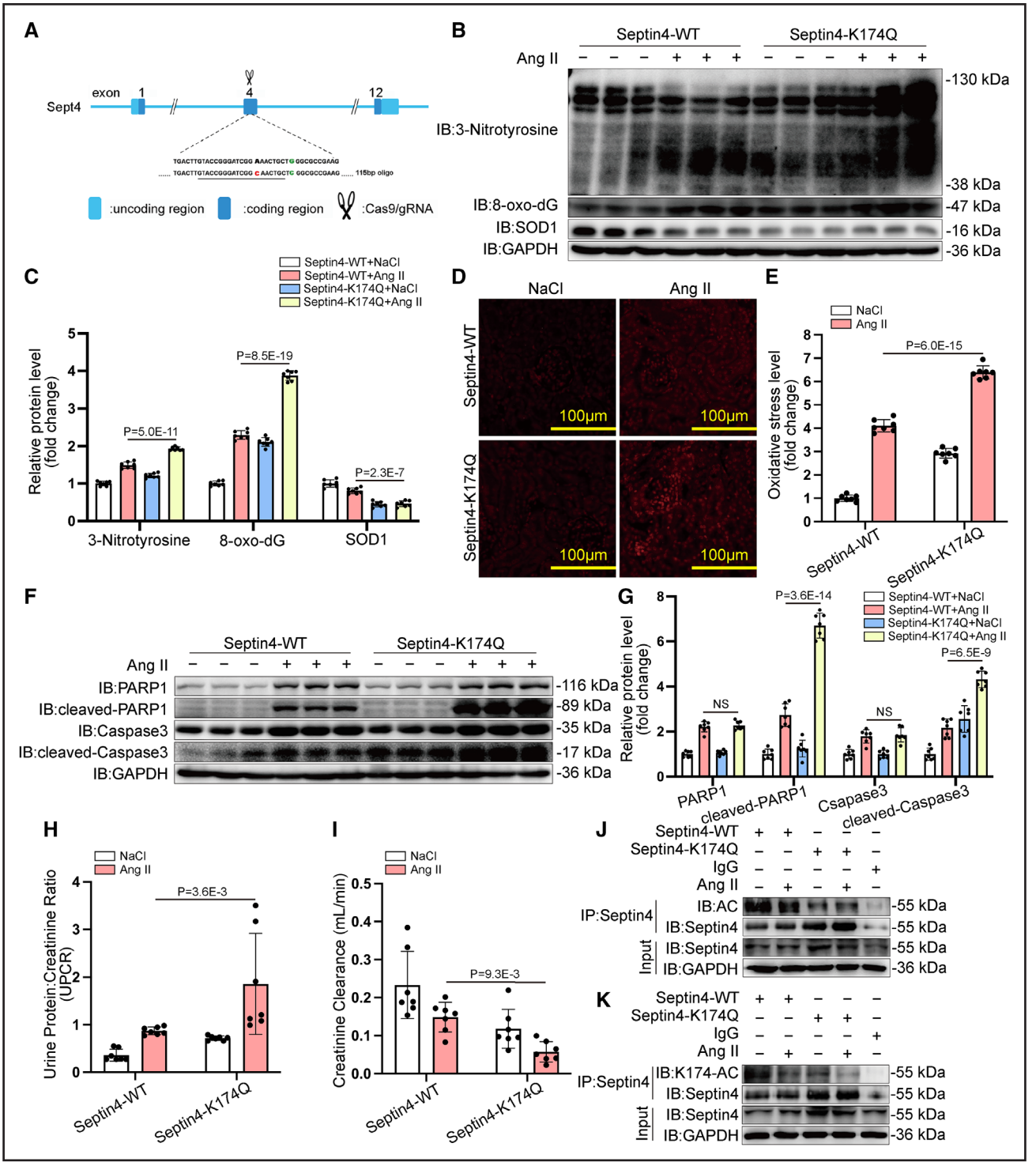

Figure 6. Septin4-K174Q significantly aggravates Ang II (angiotensin II)–induced hypertensive renal injury.
A, Diagram showing the mode of construction of *septin4*-K174Q mutant mice. Total protein was obtained from *septin4*–wild-type (WT) and *septin4*-K174Q mice renal tissue after Ang II (1.5 mg/kg per day) infusion for 14 days. **B** and **C**, Western blot was carried out to assess 3-Nitrotyrosine, 8-oxo-2'-deoxyguanosine (8-oxo-dG), and SOD1 (Superoxide Dismutase 1) expression levels. **D** and **E**, Renal tissues were stained using the DCFH-DA (2,7-Dichlorodihydrofluorescein diacetate) Assay Kit (red). Scale bar=100 μm. **F** and **G**, Western blot was carried out to assess precursors of PARP1 (poly [ADP-ribose] polymerase family, member 1) and caspase3, cleaved-PARP1, and cleaved-caspase3. **H** and **I**, Renal function was evaluated by (**H**) hour urinary protein creatinine ratio (UPCR) and (**I**) creatinine clearance (mL/min). **J** and **K**, The renal tissues were immunostained with antiseptin4 antibody and subjected to Western blot with (**J**) antiacetylation antibody (AC) and (**K**) antiseptin4-K174 acetylation antibody (K174-AC). **L** and **P**, Hematoxylin and eosin (H&E) staining was carried out to assess degree of glomerular edema. Arrowheads, renal tubular edema. Scale bar=50 μm. **M** and **Q**, AZAN (azocarmine G and anline blue) trichrome staining was carried out to assess content of extracellular matrix secretion in glomeruli. Arrowheads, extracellular matrix of glomerulus (blue). Scale bar=20 μm. **N** and **R**, (*Continued*)

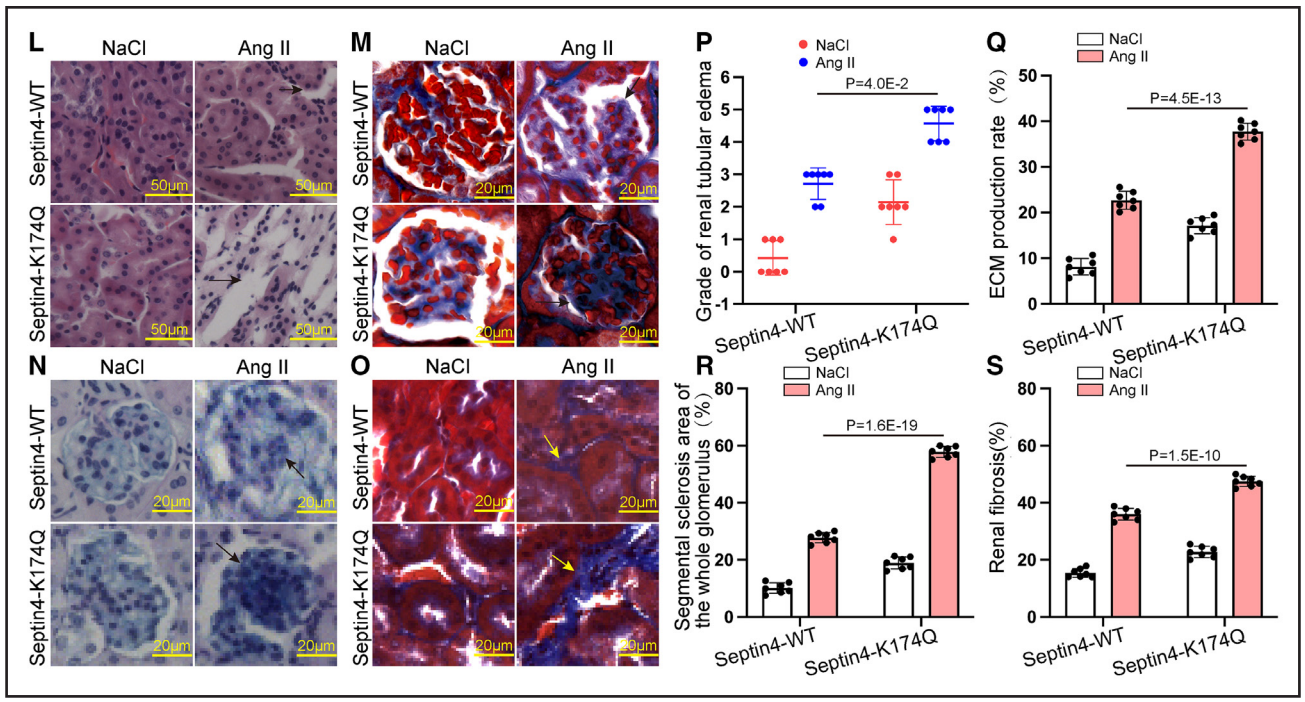

Figure 6. Continued AB-PAS (alcian blue-periodic acid schiff) staining was carried out to assess glomerular sclerosis Arrowheads, segmental sclerosis of glomerulus (lilac color). Scale bar=20 μm. **O** and **S**, Masson staining was carried out to assess degree of glomerular fibrosis. Arrowheads, glomerular fibrosis (blue). Scale bar=20 μm. **B**–**I**, **L**–**S**, For data with normality and equal variance, 2-way ANOVA with Bonferroni test was used to compare groups. If normality or homogeneity of variance was not met, treatment differences were assessed by Kruskal-Wallis test with Dunn multiple comparisons test (n=7 mice per group). Relative protein levels were calculated as fold changes vs the first group. Quantification of Western blot data is shown as mean±SD. Statistical significance was assessed by 2-way ANOVA with Bonferroni multiple comparisons test (**C**, **E**, **G**, **Q**–**S**, *P* values adjusted for 6 comparisons); Kruskal-Wallis with Dunn multiple comparisons test (**H**, **I**, **P**, *P* values adjusted for 1 comparison). IB indicates immunoblotting; and NS, not statistically significant.

mice via immunoprecipitation using a K174 sequence-specific antibody (Figure 6K). Ang II infusion for 2 weeks via osmotic minipumps was used to establish an in vivo hypertensive renal injury model in WT-*septin4* and *septin4*-K174Q mice.

We then performed proteomic analysis of the renal tissue from WT-*septin4* and *septin4*-K174Q mice induced by Ang II. Tissues were digested with trypsin followed by liquid chromatography-tandem mass spectrometry (LC-MS/MS) and bioinformatic analysis (Figure 5A). Biological replicates showed the expected correlation and repeatability at the proteomic level by Pearson correlation analysis and relative SD, and WT and septin4-K174Q are clearly distinguished by Principal Component Analysis and relative SD (Figure S5A through S5C). A total of 5650 proteins were identified by 4-dimensiaonal label-free high-depth proteomics, of which 4797 proteins had quantitative information (Figure S5D). We compared the *septin4*-K174Q and WT-*septin4* groups induced by Ang II and found 5526 common proteins between them; 72 proteins were unique to the *septin4*-K174Q group, and 53 were unique to WT-*septin4* (Figure 5B, Figure S5D). A comparison of *septin4*-K174Q samples with the corresponding WT tissues revealed 1008 proteins with statistical differences ($P<0.05$ and fold-change >1.2), of which 557 were upregulated and 451 were downregulated (Figure 5C). Differentially expressed proteins ($P<0.05$ and fold-change >1.2) in *septin4*-K174Q and WT-*septin4* mice, as compared with corresponding WT mice, are shown in volcano plots (Figure 5D).

Functional annotation, enrichment analysis, and visualization of differential proteins (fold-change>1.2, $P<0.05$) were performed among the comparison groups. In terms of Gene Ontology, more proteins are involved in cellular process, metabolic process, binding, and catalytic activity (Figure 5E). The relatively abundant proteins are localized to cytoplasm, nucleus, extracellular, mitochondria, or plasma membrane (Figure 5F). KEGG pathway analysis (Figure 5G and 5H) showed many of the upregulated proteins are in the Necroptosis pathway (Fisher exact test $P=4.32\times10^{-2}$; Figure 5I), including PARP1 (fold-change, 1.42, $P=2.17\times^{-3}$), and downstream proteins, such as Glu1 (Glutamate Synthase 1), Camk2d (Calcium/Calmodulin Dependent Protein Kinase II Delta), Pygb (Glycogen Phosphorylase, Brain Form), Pygl (Glycogen Phosphorylase, Liver Form), Pygm (Glycogen Phosphorylase, Muscle Form), of apoptosis were also upregulated. Although the proteomics analysis did not show enrichment in the apoptosis pathway, Western blot analysis of cleaved-caspase3, a key protein of apoptosis, showed that septin4-K174Q increased expression of cleaved-caspase 3 (Figure 6F).

ORIGINAL RESEARCH

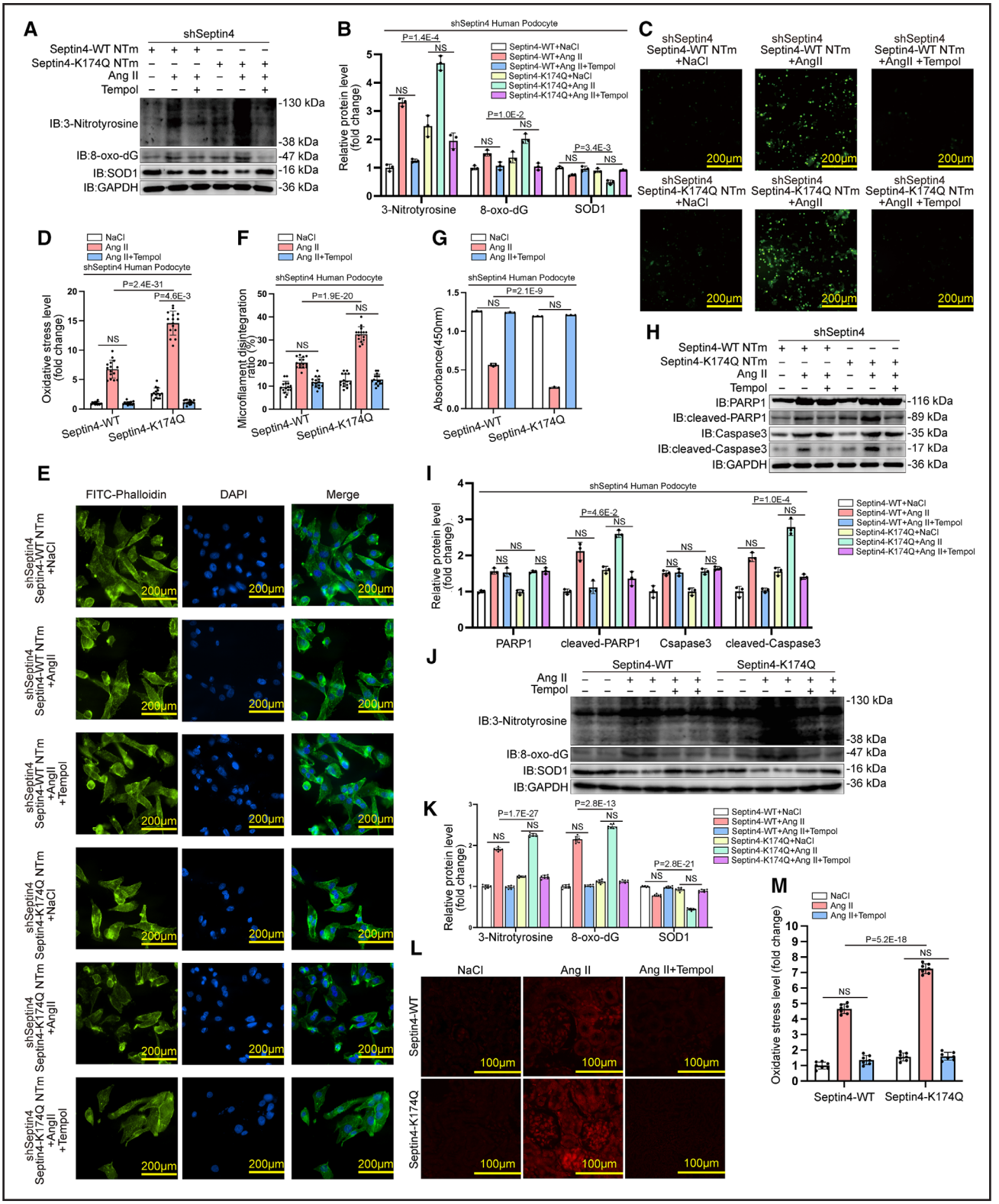

Figure 7. Oxidative stress induced by septin4-K174Q is a cause of renal podocyte apoptosis and hypertensive kidney damage. **A** and **B**, Flag-tagged *septin4* wild-type (WT)–NTm (a shRNA nontargetable mutant WT-*septin4* rescue plasmid) or K174Q-NTm plasmid was transfected into renal podocyte cells–stable septin4 knockdown (shSeptin4) cells. Renal podocyte cells were pretreated with Tempol for 12 hours and then cotreated with NaCl or 10^{-5} mol/L Ang II (angiotensin II) for 48 hours. 3-Nitrotyrosine, 8-oxo-2'-deoxyguanosine (8-oxo-dG) and SOD1 (Superoxide Dismutase 1) was assessed by Western blot (n=3 independent experiments). **C**, Renal podocyte cells were stained to detect DCFH-DA (2,7-Dichlorodihydrofluorescein diacetate) Assay Kit (green). Scale bar=200 μm. **D**, The levels of oxidative stress were measured in 5 randomly selected fluorescence microscopic visual fields in each of three independent repeated experiments (n=15). **E**, Renal podocyte cells were stained with anti-phalloidin-FITC (green) antibody. The nuclei were stained with DAPI (blue). Scale bar=200 μm. **F**, (*Continued*)

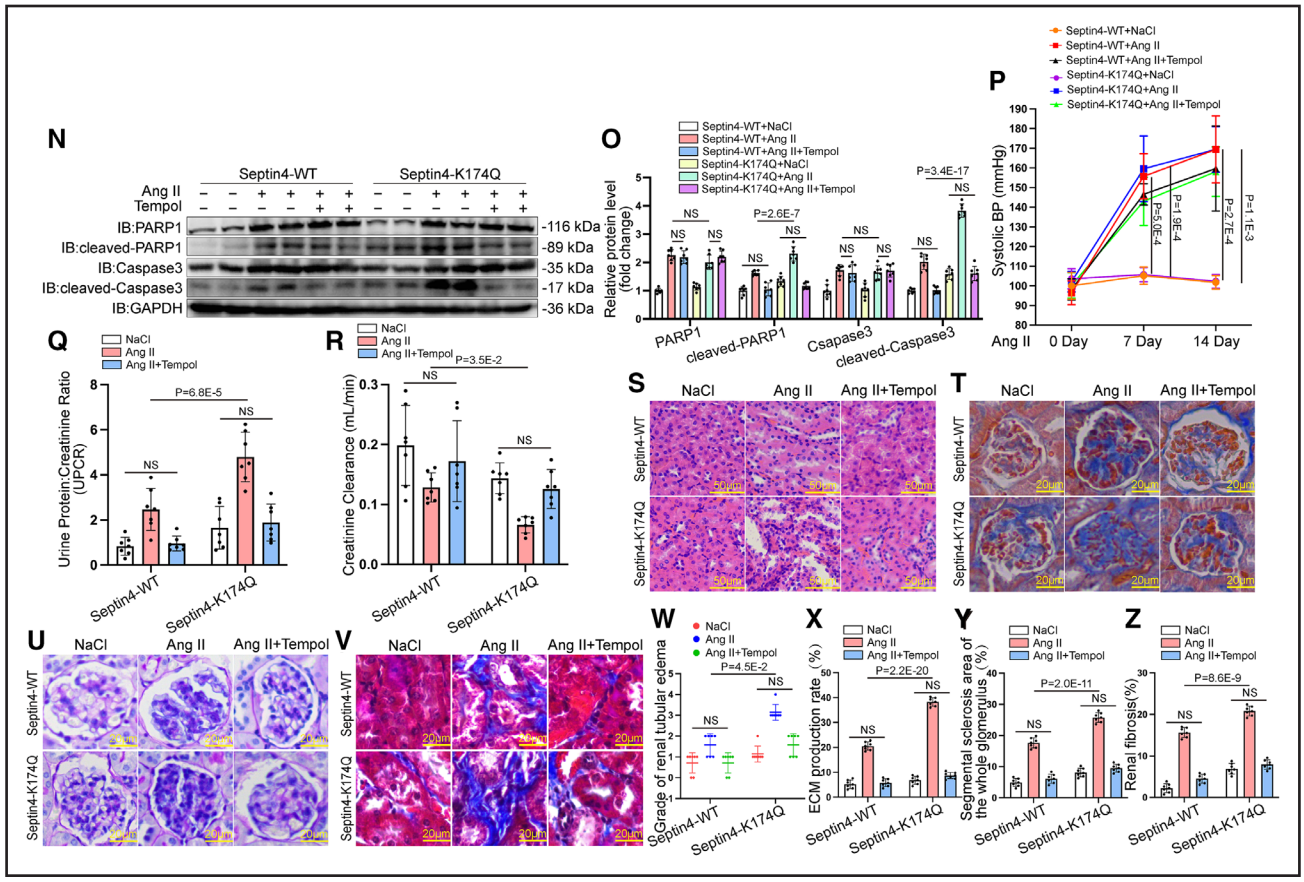

Figure 7. Continued The cells of cytoskeleton disintegration were counted in 5 randomly selected fluorescence microscopic visual fields in each of three independent experiments (n=15). **G**, Renal podocyte cell viability was measured by the CCK8 (Cell Counting Kit-8) assay (n=3 independent experiments). **H** and **I**, Flag-tagged septin4 WT-NTm or K174Q-NTm plasmid was transfected into renal podocyte cells-shSeptin4 cells. Renal podocyte cells were pretreated with Tempol for 12 hours and then cotreated with NaCl or 10^{-5} mol/L Ang II for 48 hours. The precursors of PARP1 (poly [ADP-ribose] polymerase family, member 1) and caspase3, cleaved-PARP1, and cleaved caspase3 were assessed by Western blotting. **J** and **K**, Pretreatment with Tempol (2 mmol/L in drinking water each day) continued for 7 consecutive days. Nacl or Ang II (1.5 mg/kg per day) was infused in *septin4*-WT and *septin4*-K174Q mutant mice with or without Tempol in drinking water. Western blot analysis was carried out to assess 3-nitrotyrosine, 8-oxo-dG, and SOD1 expression levels. **L** and **M**, Renal tissues were stained to detect DCFH-DA (2,7-Dichlorodihydrofluorescein diacetate) Assay Kit (red). Scale bar=100 μm. **N** and **O**, Western blot analysis was carried out to assess precursors of PARP1 and caspase3, cleaved-PARP1 and cleaved-caspase3. **P**, The blood pressure of WT and *septin4*-K174Q mice with or without Tempol pretreatment and with NaCl or Ang II were measured on days 7 and 14 by the tail-cuff method. **Q** and **R**, Renal function was evaluated by (**Q**) hour urinary protein creatinine ratio (UPCR) and (**R**) creatinine clearance (mL/min). **S** and **W**, Hematoxylin and eosin (H&E) staining was carried out to assess the degree of glomerular edema. Arrowheads, renal tubular edema. Scale bar=50 μm. **T** and **X**, AZAN (azocarmine G and anline blue) trichrome staining was carried out to assess the content of extracellular matrix secretions in glomeruli. Arrowheads, extracellular matrix of glomerulus (blue). Scale bar=20 μm. **U** and **Y**, AB-PAS (alcian blue-periodic acid Schiff) staining was carried out to assess glomerular sclerosis. Arrowheads, segmental sclerosis of glomerulus (lilac color). Scale bar=20 μm. **V** and **Z**, Masson staining was carried out to assess degree of glomerular fibrosis. Arrowheads, glomerular fibrosis (blue). Scale bar=20 μm. Three independent experiments were performed. Based on the central limit theorem the data were considered to be normally distributed (**A**–**I**). For data with normality and equal variance, 2-way ANOVA with Bonferroni test was used to compare groups. If normality or homogeneity of variance was not met, treatment differences were assessed by Kruskal-Wallis test with Dunn multiple comparisons test (n=7 mice per group; **J**–**Z**). Relative protein levels were calculated as fold changes vs the first group. Quantitated data are means±SD. Statistical significance was assessed by 2-way ANOVA with Bonferroni multiple comparisons test (**B**, **D**, **F**, **G**, **I**, **K**, **M**, **O**, **Q**, **X**–**Z**, *P* values adjusted for 15 comparisons); Kruskal-Wallis with Dunn multiple comparisons test (**P**, *P* values adjusted for 2 comparisons; **R**, **W**, *P* values adjusted for 3 comparisons). IB indicates immunoblotting; and NS, not statistically significant.

From KEGG enrichment results of downregulated proteins, we found peroxisome (Fisher exact test $P=3.31\times10^{-16}$) was ranked as a relatively enriched pathway (Figure 5J), and the majority of the pathway proteins were downregulated including the SOD1 peroxisome marker (fold-change, 0.83, $P=1.10\times10^{-4}$). The change in expression was verified by Western blot analysis in Figure 6B.

We also purified Flag-septin4 protein from 293T cells and identified its interacting proteins by mass spectrometry analysis. We performed Gene Ontology, Biological process enrichment, Molecular function enrichment, Molecular function enrichment, and Cellular component enrichment analysis on the Septin 4 interactome (Figure S6).

Septin4-K174Q Significantly Aggravates Ang II–Induced Hypertensive Renal Injury

Ang II induction in WT and *septin4*-K174Q mice was used to establish the hypertensive renal injury model. The blood pressure of WT and *septin4*-K174Q mice increased significantly with induction by Ang II ($P<0.001$), but there was no significant difference between them (Figure S2L). Renal tissues were probed using panacetylation (Figure 6J) or acetyl-K174 site-specific antibody (Figure 6K). The acetylation level of septin4-K174Q in renal tissue was significantly lower than that of septin4-WT, further confirming that the site-specific mutation in *septin4*-K174Q mice was successfully constructed. We observed higher 3-nitrotyrosine, 8-oxo-dG, SOD1, and oxidative stress level in *septin4*-K174Q mice renal tissue in response to oxidative stress injury, compared with WT-*septin4* tissue (Figure 6B through 6E).

To assess renal tissue injury in response to apoptosis in WT-*septin4* and *septin4*-K174Q mice, we compared the level of cleaved-PARP1 and cleaved-caspase3. Although the proteomics analysis did not show enrichment in the apoptosis pathway, we found higher levels in *septin4*-K174Q mice compared with WT-*septin4* mice (Figure 6F and 6G). Moreover, the precursor levels of PARP1 and caspase3 increased with the treatment of Ang II, but there was no significant difference between the 2 groups. *Septin4*-K174Q mice thus displayed aggravated apoptosis in hypertensive renal injury. UPCR of *septin4*-K174Q mice was significantly higher than that of WT mice (Figure 6H), whereas the Creatinine Clearance (mL/min) of *septin4*-K174Q mice was significantly lower (Figure 6I). These results show that *septin4*-K174Q mice display deterioration of renal function in hypertensive renal injury.

Following Ang II–induction, H&E, and AZAN trichrome staining showed that *septin4*-K174Q mice displayed significant aggravation in the degree of renal tubular edema and an increase in the area of the glomerular mesangial matrix (Figure 6L, 6M, 6P, and 6Q). Moreover, AB-PAS and Masson staining indicated that the segmental sclerosis and fibrosis areas in *septin4*-K174Q mice were larger than those in WT mice ($P<0.001$; Figure 6N, 6O, 6R, and 6S). The above results definitively show that hyper acetylation of septin4 in the K174Q mutant significantly aggravates hypertensive renal injury.

Oxidative Stress Induced by Septin4-K174Q Is a Cause of Renal Podocyte Apoptosis and Hypertensive Kidney Damage

Although the *septin4*-K174Q acetylation mimic mice show increased oxidative stress, the functional significance remained unclear. To investigate the functional role of oxidative stress in response to septin4-K174 acetylation, we conducted in vitro and in vivo experiments using the antioxidant Tempol. We analyzed shSeptin4-renal podocytes after reexpression of WT-*septin4* NTm or K174Q *septin4* NTm, with or without pretreatment with the antioxidant Tempol, or 10^{-5} mol/L Ang II–induced oxidative stress injury of renal podocytes in vitro. After reexpression of K174Q-*septin4* NTm in shSeptin4 induced by Ang II, the level of the oxidative markers 3-nitrotyrosine, 8-oxo-dG and SOD1, and the intracellular oxidative stress injury were higher than that in shSeptin4 after reexpression of WT-*septin4* NTm. The oxidative stress injury in septin4-depleted renal podocytes with reexpression of WT-*septin4* NTm. The oxidative stress injury in septin4-depleted renal podocytes with reexpression of K174Q NTm or WT-NTm was rescued by Tempol pretreatment before induction by Ang II, and there was no significant difference between the 2 groups (Figure 7A through 7D). These results indicate that Tempol significantly rescues the damaging effects of oxidative stress by septin4-K174Q.

Similarly, the level of cleaved-PARP1 and cleaved-caspase3 and the degree of cytoskeleton disintegration induced by Ang II after reexpression of K174Q-*septin4* NTm was higher than in shSeptin4 after reexpression of WT-*septin4* NTm. The level of apoptosis and the disintegration of cytoskeleton were rescued in shSeptin4 renal podocytes with reexpression of K174Q NTm and WT-NTm by Tempol pretreatment before induction by Ang II, and there was no significant difference between the two groups (Figure 7E and 7F, 7H, and 7I). However, the precursors of PARP1 and caspase3 were not affected by Tempol (Figure 7H and 7I). Similar results were obtained using CCK8 assays (Figure 7G). These results indicate that pretreatment with the antioxidant Tempol inhibits the oxidative stress reaction and prevents renal podocyte apoptosis from occurring. Therefore, it is the increase in the oxidative stress level that causes podocyte apoptosis in vitro.

Subsequently, Ang II induction of WT and *septin4*-K174Q renal tissue with or without pretreatment with Tempol was used to establish the Tempol-pretreated hypertensive renal injury model in vivo. The blood pressure of WT and *septin4*-K174Q mice increased significantly with induction by Ang II with or without pretreatment with Tempol ($P<0.001$), with no significant difference between them (Figure 7P). We observed higher levels of 3-Nitrotyrosine, 8-oxo-dG, SOD1, and increased endogenous oxidative stress levels in *septin4*-K174Q mouse renal tissue in response to oxidative stress injury, compared with WT-*septin4* mouse renal tissue (Figure 7J through 7M). The oxidative stress injury of WT and K174Q mice was almost completely rescued by pretreatment with Tempol before induction with Ang II, and there was no significant difference between the two groups. Consistent with previous in vitro experiments, these results indicate that Tempol significantly rescues the oxidative stress damage effect of septin4-K174Q in vivo.

To assess renal tissue injury in response to apoptosis and renal function in the Tempol-pretreated hypertensive renal injury model of WT-*septin4* and *septin4*-K174Q mice, we compared the level of cleaved-PARP1, cleaved-caspase3, UPCR, and creatinine clearance (mL/min). *Septin4*-K174Q mice displayed aggravated apoptosis and deterioration of renal function in hypertensive renal injury compared with *septin4*-WT mice. The apoptosis of renal tissue and renal function of WT and K174Q mice were almost completely rescued by pretreatment with Tempol before induction with Ang II, and there was no significant difference between the two groups (Figure 7N through 7O, 7Q through 7R).

The renal tubular edema degree and the area of the glomerular mesangial matrix were observed after pretreatment of mice with Tempol before induction by Ang II. H&E and AZAN trichrome staining indicated that WT and K174Q were protected by pretreatment with Tempol (Figure 7S, 7T, 7W, and 7X), and there was no significant difference between them. Indeed, the results of AB-PAS and Masson staining indicated that the segmental sclerosis and fibrosis areas in WT and *septin4*-K174Q mice were markedly alleviated after the pretreatment of Tempol (Figure 7U, 7V, 7Y, and 7Z), and there were no significant differences. Consistent with previous results, inhibiting the occurrence of the oxidative stress reaction by Tempol prevents apoptosis of renal tissue. The above results show that oxidative stress induced by septin4-K174Q is a cause of renal podocyte apoptosis and hypertensive kidney damage.

DISCUSSION

Here, we found that knockdown of septin4 exacerbates oxidative stress damage and apoptosis in renal podocytes caused by hypertension, and reexpression septin4-K174R alleviates these responses (Figure S4). Conversely, we show that hyperacetylation of septin4 at K174 (K174Q) aggravates oxidative stress, subsequently leading to apoptosis, thus ultimately enhancing the effect of hypertensive renal injury in K174Q mice (Figures 6 and 7). Septin4 is therefore a target damage factor of apoptosis in hypertensive renal injury. Moreover, septin4 exerts this biological effect via the hyperacetylation of the K174 site. We discovered that septin4, which is an apoptosis-associated non-histone protein, is regulated by SIRT2. We further uncover the molecular mechanism by which SIRT2 affects hypertensive renal injury by regulating septin4 acetylation. SIRT2 binds to the GTPase domain of septin4, which is a target of SIRT2-dependent deacetylation via lysine 174. These observations highlight the importance of the SIRT2-septin4 axis in overcoming oxidative stress and apoptosis suggest that septin4 deacetylation at K174 provides a theoretical basis for the design of treatment options and targeted drugs.

In addition to the well-known binding of SIRT2 to tubulin[35] or heat shock 70 proteins,[39] our mass spectrometry results indicated that septin4 and PARP1 potentially interact with SIRT2 (Figure 1N, Table S2). We previously showed that SIRT2 promotes ubiquitination of PARP1 through mobilization of the E3 ubiquitin ligase WWP2 (WW domain-containing protein 2), which can relieve oxidative stress–induced vascular injury and remodeling.[25,40] Thus, septin4, as a proapoptotic protein and interacting partner of SIRT2, was our main protein of interest. septin4 was the first member of the Septin family to be discovered to have proapoptotic functions. It contains a P-loop motif (GESGLGKS; Figure 1R) that is found within the GTPase domain of septin4 and contributes to its apoptotic function.[7] Our coimmunoprecipitation (Figure 1O, 1P and 1S) and immunofluorescence colocalization of proximity ligation assay (Figure 1Q) data suggest that SIRT2 physically binds to the GTPase domain of septin4.

In the presence of various cytokines,[9,10] septin4 binds directly to XIAP (X-linked inhibitor of apoptosis protein), which is followed by caspase activation.[7,8] After the release of a series of cytokines,[9,10] the caspase cascade is amplified to induce apoptosis.[9] Others have reported that septin4 plays a crucial role in regulating caspase activation and apoptosis.[7] Moreover, septin4 is currently considered to be an important marker of organ damage. Septin4 accumulates in the brain dopaminergic cells and can cause cell death and the development of Parkinson disease.[11] Meanwhile, inhibiting the expression of septin4 may alleviate liver fibrosis in *Schistosoma japonicum* infection,[41] reduce osteoblast cytoskeleton destruction,[42] decrease hypoxia-induced cardiomyocyte apoptosis,[12] and alleviate A/R-induced cardiomyopathy.[13]

The role of septin4 in hypertensive renal damage has not been previously reported. In hypertensive renal injury of shSeptin4-human renal podocytes after reexpression WT-*septin4*, we found that the level of oxidative stress was enhanced (Figure S4A through S4D), the expression of apoptosis-related proteins cleaved-caspase3 and cleaved-PARP1 increased (Figure S4E and S4F), and the cell viability decreased (Figure S4J) along with elevated cleavage of caspase8 and caspase9 (Figure S4G and S4H). Septins are components of the cytoskeleton and can act as scaffolds for protein recruitment.[38] In shSeptin4 cells reexpressing WT-*septin4* and hyperacetylation on septin4-K174Q (K174Q) induced by Ang II, cytoskeleton collapse was also observed (Figure S4I and S4K). These results indicate that septin4 aggravates hypertensive renal podocyte apoptosis through the cleaved-PARP1-cleaved caspase3 pathway via endogenous and exogenous apoptotic pathways and by enhancing the oxidative stress response.

Epigenetic modifications such as methylation,[43] phosphorylation, ubiquitylation,[44] and glycation,[44,45] have important regulatory effects on kidney diseases, including diabetic nephropathy, chronic kidney disease, and acute kidney injury.[46] In parallel, acetylation plays an

important role in the functional regulation of kidney diseases. SIRT1 alleviates sepsis-induced acute kidney injury through Beclin1 deacetylation-mediated autophagy activation,[47] and sulfhydration of SIRT1 can attenuate diabetic nephropathy via suppression of phosphorylation and acetylation of p65 NF-κB (nuclear factor kappa-B) and STAT3.[48] Previous studies on the regulation of PTM on renal diseases mainly focused on the repair of renal tubular injury and the pathological changes of glomerular stroma and mesangium. However, PTM regulation of podocyte apoptosis is rarely reported.

Podocytes constitute the glomerular filtration barrier,[4] and podocyte apoptosis directly leads to glomerulosclerosis,[4,5] which seriously affects the prognosis of renal disease.[5] Alleviating podocyte apoptosis is key to facilitating repair after renal injury. Here, we elucidate the mechanism by which deacetylation alleviates podocyte apoptosis. In addition, our study is the first to report the role of deacetylation regulation in hypertension-induced renal injury. We find that SIRT2 shows the highest upregulation in the expression profiles of Sirtuin family members with Ang II–induced hypertensive renal damage mice (Figure 1B). We also found that the expression of SIRT2 in human hypertensive renal tissues was significantly higher than in tissues without hypertension (Figure 1C and 1D), suggesting that SIRT2 is the most significant factor in hypertensive renal injury. As an NAD+-dependent deacetylase, SIRT2 deacetylates substrates that participate in diverse processes. Increasing evidence suggests SIRT2 can inhibit oxidative stress-triggered apoptosis in cardiomyocytes[19] and tumor cells.[20] At the same time, it also plays a protective role against oxidative stress-heart failure and Ang II–induced myocardial hypertrophy.[22,23] However, the anti-apoptotic effect of SIRT2 in hypertensive renal injury was unknown. Only a few studies showed that SIRT2 may play a role in acute tubular injury.[49] We observed that in *Sirt2* knockout mice, oxidative stress (Figure 3G through 3J) and apoptosis (Figure 3K and 3L) was aggravated. UPCR increased, whereas renal function decreased (Figure 3M and 3N), and renal pathological staining was aggravated (Figure 3O through 3V) in hypertensive renal injury in *Sirt2* knockout mice. In contrast, these phenomena were alleviated in *Sirt2*-TG mice (Figure 4G through 4V). Correspondingly, in Ang II–induced SIRT2-knockdown renal podocytes, oxidative stress, and apoptosis increased, cell viability decreased, and the cytoskeleton disintegrated. Reexpression of SIRT2 rescued these injury responses (Figure S3C through S3K). Our work is the first to show SIRT2 can alleviate apoptosis of hypertensive renal injury at the cellular and animal levels.

The regulation of acetylation of apoptotic proteins is also important in the occurrence and development of diseases,[50–52] and the regulation of PTM on septin4 also plays a pivotal role in apoptosis. XIAP[15] or Parkin,[14] an E3 ubiquitin ligase, promotes the ubiquitination and degradation of septin4, thus keeping septin4 at low levels in healthy cells and preventing unnecessary apoptosis.[15] In addition, DYRK1A (dual specificity tyrosine-phosphorylation-regulated kinase 1A) specifically interacts with septin4 and phosphorylates Ser68 and/or Ser107, thereby participating in neurodegenerative processes.[16] However, the regulation of septin4 acetylation has not been reported. Using septin4-K174 site-specific antibody for immunoprecipitation, we confirmed that the K174 site of septin4 is acetylated by CBP and deacetylated by SIRT2 (Figure 2). This was also confirmed in SIRT2-knockdown cells (Figure S3B), *Sirt2* knockout mice (Figure 3E through 3F), and *Sirt2*-TG mice (Figure 4E and 4F) with hypertensive renal injury.

We established the hypertensive renal injury model using the first international *septin4*-K174Q hyperacetylated mice and analyzed them by LC-MS/MS and Bioinformatics. 4797 proteins with quantitative information were identified by 4D label-free high-depth proteomics (Figure 5C). KEGG pathway analysis (Figure 5G and 5H) showed the Necroptosis pathway, including PARP1 (fold-change, 1.42, $P=2.17\times^{-3}$; Figure 5I) and Peroxisome pathway including SOD1 (fold-change, 0.83, $P=1.10\times^{-4}$; Figure 5J) were the relatively significant downstream pathways affected in *septin4*-K174Q mice. The above results were subsequently verified by biological experiments, and these phenotypes were consistent with the observations in *Sirt2* knockout mice. Oxidative stress and apoptosis were elevated, accompanied by increasing UPCR and deterioration of renal function, with aggravated renal pathological staining in hypertensive renal injury of *septin4*-K174Q mice (Figure 6). Subsequently, we found that by using pretreatment with the antioxidant Tempol to inhibit the oxidative stress reaction in our in vivo and in vitro experiments, the renal podocyte apoptosis, cytoskeleton disintegration, and hypertensive kidney damage could not occur (Figure 7).

However, using the probe DCFH-DA to detect changes in oxidative stress marker levels has some limitations. The term "reactive oxygen species" is not a single entity, but is rather a general term for a group of reactive species with different chemical properties and biological reactivities, including superoxide ($\cdot O_2-$), hydrogen peroxide, hydroxyl radicals, and alkoxy radicals. Various fluorescent probes are used to detect intracellular reactive oxygen species. DCFH-DA is a nonfluorescent form of DCF with cell permeability and is the most widely used probe to detect intracellular H_2O_2 and oxidative stress. After entering the cytoplasm, it is cleaved by intracellular esterases into fluorescent DCF, which then reacts with various types of reactive oxygen species, especially hydroxyl radicals ($\cdot OH$). However, DCFH-DA is highly unstable with some limitations and artifacts in detection. First, DCFH-DA does not directly react with H_2O_2 and cannot directly measure H_2O_2. Second, some one-electron-oxidizing species, cytochrome c, redox-active metals, intermediate radicals DCF·and other interfering factors may lead to enhanced fluorescence

signal. Finally, since reactive oxygen species are transient within cells, especially superoxide and nitric oxide, real-time measurements are required.[53,54] Despite these limitations, we simultaneously detected changes in oxidative stress–related markers including 3-Nitrotyrosine, 8-oxo-dG, and SOD1 with Western blotting assays, and the changes of oxidative stress levels both in vivo and vitro experiments were well-documented. Therefore, the conclusion that the deacetylation of septin4-K174 by SIRT2 mitigates Ang II–induced hypertensive renal injury resulting from oxidative stress is supported by abundant evidence.

The above results show that oxidative stress induced by septin4-K174Q is a cause of renal podocyte apoptosis, cytoskeleton disintegration, and hypertensive kidney damage. We fully confirmed that hyperacetylation on septin4-K174 (K174Q) causes increased oxidative stress, thus significantly aggravating hypertensive kidney damage. Thus, SIRT2 alleviates the oxidative stress response of podocytes, the disintegration of podocyte cytoskeleton, and podocyte apoptosis through deacetylation of septin4-K174, and ultimately alleviates hypertensive renal injury in mice. These results suggest that septin4 K174R (mimicking deacetylation by SIRT2) is a potential target to confer resistance to hypertensive renal injury.

In summary, we have identified an acetylation-dependent regulatory mechanism governing septin4 in hypertensive renal injury. Septin4 acetylation aggravates Ang II–induced hypertensive renal injury. We find that septin4 may be a critical factor in SIRT2-mediated hypertensive renal injury and provide a potential mechanism by which SIRT2 acts as a protective factor in hypertensive renal injury. These observations demonstrate the potential utility of targeting septin4-K174 deacetylation for treatment of hypertensive renal injury.

ARTICLE INFORMATION

Received June 26, 2022; revision received January 22, 2023; accepted February 1, 2023.

Affiliations

Department of Cardiology (Y.Z., N.Z., Y.Z., C.S., K.C., B.W., S.Y., S.L., D.W., J.X., X.H., P.Z., Z.F., Y.S.) and Department of Urology (Z.Z., C.K.), the First Hospital of China Medical University, Shenyang, Liaoning, People's Republic of China. Institute of Health Sciences, China Medical University (Y.Z., N.Z., Y.S.). Key Laboratory of Reproductive and Genetic Medicine (China Medical University), National Health Commission, Shenyang, China (N.Z.). College of Basic Medical Science; Key Laboratory of Medical Cell Biology, Ministry of Education; Liaoning Province Collaborative Innovation Center of Aging Related Disease Diagnosis and Treatment and Prevention, Shenyang, Liaoning Province, China (J.L., L.C.). Jingjie PTM BioLab Co. Ltd (Z.C.).

Acknowledgements

We are grateful to Dr Qunying Lei, from Fudan University, Shanghai, China for providing Flag-P300, Flag-CBP (CREB binding protein), and Myc-tagged GCN5 (histone acetyltransferase GCN5) plasmids and to Dr Weiguo Zhu from Shenzhen University, Shenzhen, China, for providing Flag–PCAF (lysine acetyltransferase 2B). And we are grateful to Xinrui Meng, from Jingjie PTM BioLab Co. Ltd, China, for his help in processing the proteomics data. The mass spectrometry proteomics and acetyl proteomics data have been deposited to the ProteomeXchange Consortium (http://proteomecentral.proteomexchange.org/cgi/GetDataset?ID=PXD038538) or iProx database (https://www.iprox.cn/page/project.html?id=IPX0005536000) via the iProX partner repository with the dataset identifier PXD038538 (project ID: IPX0005536000).

Sources of Funding

This work was supported by Natural Science Foundation of China (81900372, 82171571, 82171572, 81970211 and 81900355, 82102740).

Disclosures

None.

Supplemental Material

Supplemental Methods
Figures S1–S6
Tables S1–S4
References 31, 55, 56

REFERENCES

1. Visseren FLJ, Mach F, Smulders YM, Carballo D, Koskinas KC, Bäck M, Benetos A, Biffi A, Boavida J-M, Capodanno D, et al; ESC National Cardiac Societies. 2021 esc guidelines on cardiovascular disease prevention in clinical practice. *Eur Heart J*. 2021;42:3227–3337. doi: 10.1093/eurheartj/ehab484
2. GBD 2017 Disease and Injury Incidence and Prevalence Collaborators. Global, regional, and national incidence, prevalence, and years lived with disability for 354 diseases and injuries for 195 countries and territories, 1990-2017: a systematic analysis for the global burden of disease study 2017. *Lancet*. 2018;392:1789–1858. doi: 10.1016/S0140-6736(18)32279-7
3. Wei S-Y, Wang Y-X, Zhang Q-F, Zhao S-L, Diao T-T, Li J-S, Qi W-R, He Y-X, Guo X-Y, Zhang M-Z, et al. Multiple mechanisms are involved in salt-sensitive hypertension-induced renal injury and interstitial fibrosis. *Sci Rep*. 2017;7:45952. doi: 10.1038/srep45952
4. Nagase M, Shibata S, Yoshida S, Nagase T, Gotoda T, Fujita T. Podocyte injury underlies the glomerulopathy of dahl salt-hypertensive rats and is reversed by aldosterone blocker. *Hypertension*. 2006;47:1084–1093. doi: 10.1161/01.HYP.0000222003.28517.99
5. Shankland SJ. The podocyte's response to injury: role in proteinuria and glomerulosclerosis. *Kidney Int*. 2006;69:2131–2147. doi: 10.1038/sj.ki.5000410
6. Kretzler M, Koeppen-Hagemann I, Kriz W. Podocyte damage is a critical step in the development of glomerulosclerosis in the uninephrectomised-desoxycorticosterone hypertensive rat. *Virchows Arch*. 1994;425:181–193. doi: 10.1007/BF00230355
7. Larisch S, Yi Y, Lotan R, Kerner H, Eimerl S, Tony Parks W, Gottfried Y, Birkey Reffey S, de Caestecker MP, Danielpour D, et al. A novel mitochondrial septin-like protein, arts, mediates apoptosis dependent on its p-loop motif. *Nat Cell Biol*. 2000;2:915–921. doi: 10.1038/35046566
8. Gottfried Y, Rotem A, Lotan R, Steller H, Larisch S. The mitochondrial arts protein promotes apoptosis through targeting xiap. *EMBO J*. 2004;23:1627–1635. doi: 10.1038/sj.emboj.7600155
9. Edison N, Zuri D, Maniv I, Bornstein B, Lev T, Gottfried Y, Kemeny S, Garcia-Fernandez M, Kagan J, Larisch S. The iap-antagonist arts initiates caspase activation upstream of cytochrome c and smac/diablo. *Cell Death Differ*. 2012;19:356–368. doi: 10.1038/cdd.2011.112
10. Edison N, Curtz Y, Paland N, Mamriev D, Chorubczyk N, Haviv-Reingewertz T, Kfir N, Morgenstern D, Kupervaser M, Kagan J, et al. Degradation of bcl-2 by xiap and arts promotes apoptosis. *Cell Rep*. 2017;21:442–454. doi: 10.1016/j.celrep.2017.09.052
11. Muñoz-Soriano V, Nieto-Arellano R, Paricio N. Septin 4, the drosophila ortholog of human cdcrel-1, accumulates in parkin mutant brains and is functionally related to the nedd4 e3 ubiquitin ligase. *J Mol Neurosci*. 2012;48:136–143. doi: 10.1007/s12031-012-9788-3
12. Wu S, Zhang Y, You S, Lu S, Zhang N, Sun Y. Septin4 promotes cardiomyocytes apoptosis by enhancing the vhl-mediated degradation of hif-1α. *Cell Death Discov*. 2021;7:172. doi: 10.1038/s41420-021-00563-4
13. Song Y, Ren X, Gao F, Li F, Zhou J, Chen J, Zhang Y. Linc01588 regulates wwp2-mediated cardiomyocyte injury by interacting with hnrnpl. *Environ Toxicol*. 202237:1629. doi: 10.1002/tox.23512
14. Kemeny S, Dery D, Loboda Y, Rovner M, Lev T, Zuri D, Finberg JP, Larisch S. Parkin promotes degradation of the mitochondrial pro-apoptotic arts protein. *PLoS One*. 2012;7:e38837. doi: 10.1371/journal.pone.0038837
15. Bornstein B, Edison N, Gottfried Y, Lev T, Shekhtman A, Gonen H, Rajalingam K, Larisch S. X-linked inhibitor of apoptosis protein promotes the

degradation of its antagonist, the pro-apoptotic arts protein. *Int J Biochem Cell Biol*. 2012;44:489–495. doi: 10.1016/j.biocel.2011.12.005
16. Sitz JH, Baumgärtel K, Hämmerle B, Papadopoulos C, Hekerman P, Tejedor FJ, Becker W, Lutz B. The down syndrome candidate dual-specificity tyrosine phosphorylation-regulated kinase 1a phosphorylates the neurodegeneration-related septin 4. *Neuroscience*. 2008;157:596–605. doi: 10.1016/j.neuroscience.2008.09.034
17. Bonkowski MS, Sinclair DA. Slowing ageing by design: the rise of nad and sirtuin-activating compounds. *Nat Rev Mol Cell Biol*. 2016;17:679–690. doi: 10.1038/nrm.2016.93
18. Braunstein M, Rose AB, Holmes SG, Allis CD, Broach JR. Transcriptional silencing in yeast is associated with reduced nucleosome acetylation. *Genes Dev*. 1993;7:592–604. doi: 10.1101/gad.7.4.592
19. Katare PB, Nizami HL, Paramesha B, Dinda AK, Banerjee SK. Activation of toll like receptor 4 (tlr4) promotes cardiomyocyte apoptosis through sirt2 dependent p53 deacetylation. *Sci Rep*. 2020;10:19232. doi: 10.1038/s41598-020-75301-4
20. Peck B, Chen C-Y, Ho K-K, Di Fruscia P, Myatt SS, Coombes RC, Fuchter MJ, Hsiao C-D, Lam EWF. Sirt inhibitors induce cell death and p53 acetylation through targeting both sirt1 and sirt2. *Mol Cancer Ther*. 2010;9:844–855. doi: 10.1158/1535-7163.MCT-09-0971
21. Liu G, Park S-H, Imbesi M, Nathan WJ, Zou X, Zhu Y, Jiang H, Parisiadou L, Gius D. Loss of nad-dependent protein deacetylase sirtuin-2 alters mitochondrial protein acetylation and dysregulates mitophagy. *Antioxid Redox Signal*. 2017;26:849–863. doi: 10.1089/ars.2016.6662
22. Sarikhani M, Maity S, Mishra S, Jain A, Tamta AK, Ravi V, Kondapalli MS, Desingu PA, Khan D, Kumar S, et al. Sirt2 deacetylase represses nfat transcription factor to maintain cardiac homeostasis. *J Biol Chem*. 2018;293:5281–5294. doi: 10.1074/jbc.RA117.000915
23. Tang X, Chen X-F, Wang N-Y, Wang X-M, Liang S-T, Zheng W, Lu Y-B, Zhao X, Hao D-L, Zhang Z-Q, et al. Sirt2 acts as a cardioprotective deacetylase in pathological cardiac hypertrophy. *Circulation*. 2017;136:2051–2067. doi: 10.1161/CIRCULATIONAHA.117.028728
24. Peterson AC, Russell JD, Bailey DJ, Westphall MS, Coon JJ. Parallel reaction monitoring for high resolution and high mass accuracy quantitative, targeted proteomics. *Mol Cell Proteomics*. 2012;11:1475–1188. doi: 10.1074/mcp.O112.020131
25. Zhang N, Zhang Y, Wu B, Wu S, You S, Lu S, Liu J, Huang X, Xu J, Cao L, et al. Deacetylation-dependent regulation of parp1 by sirt2 dictates ubiquitination of parp1 in oxidative stress-induced vascular injury. *Redox Biol*. 2021;47:102141. doi: 10.1016/j.redox.2021.102141
26. Ekwall K, Olsson T, Turner BM, Cranston G, Allshire RC. Transient inhibition of histone deacetylation alters the structural and functional imprint at fission yeast centromeres. *Cell*. 1997;91:1021–1032. doi: 10.1016/s0092-8674(00)80492-4
27. Furumai R, Komatsu Y, Nishino N, Khochbin S, Yoshida M, Horinouchi S. Potent histone deacetylase inhibitors built from trichostatin a and cyclic tetrapeptide antibiotics including trapoxin. *Proc Natl Acad Sci U S A*. 2001;98:87–92. doi: 10.1073/pnas.98.1.87
28. Avalos JL, Bever KM, Wolberger C. Mechanism of sirtuin inhibition by nicotinamide: Altering the nad(+) cosubstrate specificity of a sir2 enzyme. *Mol Cell*. 2005;17:855–868. doi: 10.1016/j.molcel.2005.02.022
29. Outeiro TF, Kontopoulos E, Altmann SM, Kufareva I, Strathearn KE, Amore AM, Volk CB, Maxwell MM, Rochet J-C, McLean PJ, et al. Sirtuin 2 inhibitors rescue alpha-synuclein-mediated toxicity in models of parkinson's disease. *Science*. 2007;317:516–519. doi: 10.1126/science.1143780
30. Villalba JM, Alcaín FJ. Sirtuin activators and inhibitors. *Biofactors*. 2012;38:349–359. doi: 10.1002/biof.1032
31. Kim H-S, Vassilopoulos A, Wang R-H, Lahusen T, Xiao Z, Xu X, Li C, Veenstra TD, Li B, Yu H, et al. Sirt2 maintains genome integrity and suppresses tumorigenesis through regulating apc/c activity. *Cancer Cell*. 2011;20:487–499. doi: 10.1016/j.ccr.2011.09.004
32. Reidy K, Kang HM, Hostetter T, Susztak K. Molecular mechanisms of diabetic kidney disease. *J Clin Invest*. 2014;124:2333–2340. doi: 10.1172/JCI72271
33. Oshima M, Shimizu M, Yamanouchi M, Toyama T, Hara A, Furuichi K, Wada T. Trajectories of kidney function in diabetes: a clinicopathological update. *Nat Rev Nephrol*. 2021;17:740–750. doi: 10.1038/s41581-021-00462-y
34. Chen B-C, Shibu MA, Kuo C-H, Shen C-Y, Chang-Lee SN, Lai C-H, Chen R-J, Yao C-H, Viswanadha VP, Liu J-S, et al. E4bp4 inhibits angii-induced apoptosis in h9c2 cardiomyoblasts by activating the pi3k-akt pathway and promoting calcium uptake. *Exp Cell Res*. 2018;363:227–234. doi: 10.1016/j.yexcr.2018.01.012
35. North BJ, Marshall BL, Borra MT, Denu JM, Verdin E. The human sir2 ortholog, sirt2, is an nad+-dependent tubulin deacetylase. *Mol Cell*. 2003;11:437–444. doi: 10.1016/s1097-2765(03)00038-8
36. Wang Y, Yang J, Hong T, Chen X, Cui L. Sirt2: controversy and multiple roles in disease and physiology. *Ageing Res Rev*. 2019;55:100961. doi: 10.1016/j.arr.2019.100961
37. Nagata S. Apoptosis and clearance of apoptotic cells. *Annu Rev Immunol*. 2018;36:489–517. doi: 10.1146/annurev-immunol-042617-053010
38. Mostowy S, Cossart P. Septins: the fourth component of the cytoskeleton. *Nat Rev Mol Cell Biol*. 2012;13:183–194. doi: 10.1038/nrm3284
39. Hageman J, Rujano MA, van Waarde MAWH, Kakkar V, Dirks RP, Govorukhina N, Oosterveld-Hut HMJ, Lubsen NH, Kampinga HH. A dnajb chaperone subfamily with hdac-dependent activities suppresses toxic protein aggregation. *Mol Cell*. 2010;37:355–369. doi: 10.1016/j.molcel.2010.01.001
40. Zhang N, Zhang Y, Qian H, Wu S, Cao L, Sun Y. Selective targeting of ubiquitination and degradation of parp1 by e3 ubiquitin ligase wwp2 regulates isoproterenol-induced cardiac remodeling. *Cell Death Differ*. 2020;27:2605–2619. doi: 10.1038/s41418-020-0523-2
41. Zhu D, Song K, Chen J, Wang J, Sun X, Qian H, Gu X, Zhang L, Qin Y, Duan Y. Expression of septin4 in schistosoma japonicum-infected mouse livers after praziquantel treatment. *Parasit Vectors*. 2015;8:19. doi: 10.1186/s13071-015-0640-9
42. Tao L, Zhao S, Tao Z, Wen K, Zhou S, Da W, Zhu Y. Septin4 regulates endoplasmic reticulum stress and apoptosis in melatonin-induced osteoblasts. *Mol Med Rep*. 2020;22:1179–1186. doi: 10.3892/mmr.2020.11228
43. Kato M, Natarajan R. Epigenetics and epigenomics in diabetic kidney disease and metabolic memory. *Nat Rev Nephrol*. 2019;15:327–345. doi: 10.1038/s41581-019-0135-6
44. Yang X, Okamura DM, Lu X, Chen Y, Moorhead J, Varghese Z, Ruan XZ. Cd36 in chronic kidney disease: Novel insights and therapeutic opportunities. *Nat Rev Nephrol*. 2017;13:769–781. doi: 10.1038/nrneph.2017.126
45. Rabbani N, Thornalley PJ. Advanced glycation end products in the pathogenesis of chronic kidney disease. *Kidney Int*. 2018;93:803–813. doi: 10.1016/j.kint.2017.11.034
46. Guo C, Dong G, Liang X, Dong Z. Epigenetic regulation in aki and kidney repair: Mechanisms and therapeutic implications. *Nat Rev Nephrol*. 2019;15:220–239. doi: 10.1038/s41581-018-0103-6
47. Deng Z, Sun M, Wu J, Fang H, Cai S, An S, Huang Q, Chen Z, Wu C, Zhou Z, et al. Sirt1 attenuates sepsis-induced acute kidney injury via beclin1 deacetylation-mediated autophagy activation. *Cell Death Dis*. 2021;12:217. doi: 10.1038/s41419-021-03508-y
48. Sun H-J, Xiong S-P, Cao X, Cao L, Zhu M-Y, Wu Z-Y, Bian J-S. Polysulfide-mediated sulfhydration of sirt1 prevents diabetic nephropathy by suppressing phosphorylation and acetylation of p65 nf-κb and stat3. *Redox Biol*. 2021;38:101813. doi: 10.1016/j.redox.2020.101813
49. Jung YJ, Lee AS, Nguyen-Thanh T, Kim D, Kang KP, Lee S, Park SK, Kim W. Sirt2 regulates lps-induced renal tubular cxcl2 and ccl2 expression. *J Am Soc Nephrol*. 2015;26:1549–1560. doi: 10.1681/ASN.2014030226
50. Wang Z, Sun R, Wang G, Chen Z, Li Y, Zhao Y, Liu D, Zhao H, Zhang F, Yao J, et al. Sirt3-mediated deacetylation of prdx3 alleviates mitochondrial oxidative damage and apoptosis induced by intestinal ischemia/reperfusion injury. *Redox Biol*. 2020;28:101343. doi: 10.1016/j.redox.2019.101343
51. Terui T, Murakami K, Takimoto R, Takahashi M, Takada K, Murakami T, Minami S, Matsunaga T, Takayama T, Kato J, et al. Induction of pig3 and noxa through acetylation of p53 at 320 and 373 lysine residues as a mechanism for apoptotic cell death by histone deacetylase inhibitors. *Cancer Res*. 2003;63:8948–8954.
52. Liu R, Zhong Y, Li X, Chen H, Jim B, Zhou M-M, Chuang PY, He JC. Role of transcription factor acetylation in diabetic kidney disease. *Diabetes*. 2014;63:2440–2453. doi: 10.2337/db13-1810
53. Gardiner B, Dougherty JA, Ponnalagu D, Singh H, Angelos M, Chen CA, Khan M. Measurement of oxidative stress markers in vitro using commercially available kits. In: Berliner LJ, Parinandi NL, eds. *Measuring oxidants and oxidative stress in biological systems*. Springer Copyright 2020, Springer Nature Switzerland AG.; 2020:39–60.
54. Kalyanaraman B, Darley-Usmar V, Davies KJ, Dennery PA, Forman HJ, Grisham MB, Mann GE, Moore K, Roberts LJ 2nd, Ischiropoulos H. Measuring reactive oxygen and nitrogen species with fluorescent probes: challenges and limitations. *Free Radic Biol Med*. 2012;52:1–6. doi: 10.1016/j.freeradbiomed.2011.09.030
55. Caroccia B, Seccia TM, Barton M, Rossi GP. Estrogen signaling in the adrenal cortex: Implications for blood pressure sex differences. *Hypertension*. 2016;68:840–848. doi: 10.1161/HYPERTENSIONAHA.116.07660
56. Zhang Y, Yi F, Wang L, Wang Z, Zhang N, Wang Z, Li Z, Song X, Wei S, Cao L. Phosphorylation of smc1a promotes hepatocellular carcinoma cell proliferation and migration. *Int J Biol Sci*. 2018;14:1081–1089. doi: 10.7150/ijbs.24692